CHALMERS
UNIVERSITY OF TECHNOLOGY

Simulation of charging behavior on surfaces of polymeric insulation inside HVAC cable termination

Master's thesis in Electric Power Engineering

CHENXUAN SUN

Department of Electrical Engineering
CHALMERS UNIVERSITY OF TECHNOLOGY
Gothenburg, Sweden 2020

Master's thesis

Simulation of charging behavior on surfaces of polymeric insulation inside HVAC cable termination

CHENXUAN SUN

CHALMERS
UNIVERSITY OF TECHNOLOGY

Department of Electrical Engineering
Division of Electric Power Engineering
Chalmers University of Technology
Gothenburg, Sweden 2020

Simulation of charging behavior on surfaces of polymeric insulation inside HVAC cable termination
Chenxuan Sun

Supervisor: Adjunct Professor Olof Hjortstam, Hitachi ABB Power Grids Research
Examiner: Professor Yuriy Serdyuk, Department of Electrical Engineering

Master's Thesis
Department of Electrical Engineering
Division of Electric Power Engineering
Chalmers University of Technology
SE-412 96 Gothenburg
Telephone +46 31 772 1000

Typeset in LaTeX
Gothenburg, Sweden 2020

Simulation of charging behavior on surfaces of polymeric insulation inside HVAC cable termination

Chenxuan Sun
Department of Electrical Engineering
Chalmers University of Technology

Abstract

Electrical energy systems are easily exposed to atmospheric lightnings and suffer from extreme high dielectric strength which will result in failures in insulating materials. A model describing charge and discharge behaviours along polymeric surface in a HVAC cable termination under lightning impulses is implemented in COMSOL Multiphysics. The drift and diffusion of charged molecular are described by partial differential equations which is coupled with Poisson's equation for computing charge-dominated electric field. Various simulations are conducted to evaluate the impacts of voltage levels, voltage polarities, gel heights, decay of surface charges and numbers of impulses on corona discharges.

The results show that the higher voltage levels and gel heights will result in more intensive discharges and the voltage polarities will affect the developments of corona discharges and have different impacts for insulating materials. The accumulation of surface charges is observed between impulses that with more impulse applied higher amount of surface charges is collected and thus intensify the discharges in following impulses. The decay of surface charge between impulses is analyzed with the constraints of computational power and time for supplementing the discussion.

Keywords: Corona discharge, surface charge, charge accumulation, lightning impulse voltage, high voltage, HVAC cable termination, FEM simulation.

Acknowledgements

I would like to show my sincere appreciation to my supervisor, Adjunct Professor Olof Hjortstam, for providing enormous support throughout the project. Olof patiently introduced the topics, built up a good framework for the project and offered valuable advice. The project would not be possible without his support.

I also want to pay my special regards to my examiner, Professor Yuriy Serdyuk, who gave valuable comments on the simulation work and shared his knowledge unconditionally. He also provides the remote access of the working station which has been a great help to the work.

Besides, I wish to show my gratitude to Doctor Chen Lei and Doctor David Kiefer from NKT HV Cable, for their offering for help and hospitality of showing the factory and products. The information they provided has been important inputs for the work. Also, I would like to thank Philip Hoang for the good discussion related to the topic throughout the project.

Finally, special thanks to my families and friends for their support and understanding. And gratitude to all the key workers battling the COVID-19 pandemic.

Chenxuan Sun, Gothenburg, June 2020

Contents

List of Figures **xi**

List of Tables **xv**

1 Introduction **1**
1.1 Background . . . 1
1.2 Aim . . . 2
1.3 Problem . . . 2
1.4 Scope . . . 3
1.5 Sustainability and ethical aspects . . . 3

2 Fundamental physical processes in gas discharges **5**
2.1 Generation and losses of charge carriers . . . 5
2.2 Transport of charged species due to drift and diffusion . . . 7
2.3 Hydrodynamic description of charge motion . . . 7
2.4 Space charges and surface charges accumulation on interfaces . . . 8
2.5 Main stages of discharge development . . . 9
2.6 Discharge current . . . 10

3 The model and computer implementation **13**
3.1 Geometry and materials . . . 13
3.2 Multiphysics aspects . . . 15
3.2.1 Poisson's equation and calculations of the electric field . . . 15
3.2.2 Charge transport equations . . . 15
3.2.3 Surface charges accumulation . . . 16
3.3 Model coefficients, parameters and variables . . . 17
3.4 Finite element mesh . . . 21
3.5 Calculations of the discharge current . . . 22

4 Results and Discussion **25**
4.1 1D Model . . . 25
4.1.1 Corona Discharge . . . 26
4.1.2 Stabilization method . . . 31
4.2 2D model . . . 34
4.2.1 2D model with a rounded triple junction . . . 34
4.2.1.1 Corona discharge in 2D model . . . 35
4.2.1.2 Influence of voltage level and gel height . . . 38

4.2.1.3 Influence of voltage polarity 41
4.2.1.4 Conclusion 43
4.2.2 Scaled-down 2D model 45
4.2.2.1 Field reversal 46
4.2.2.2 Consecutive lightning impulses 48
4.2.2.3 Surface charge decay 52
4.2.2.4 Gel height and voltage polarity 54
4.2.2.5 Conclusion 55
4.3 Discussion and interpretation 57

5 Conclusion **59**
5.1 Main findings 59
5.2 Future work 59

Bibliography **61**

A Appendix **I**

List of Figures

1.1 *Static calculation of electric field strength inside the cable termination. The triple junction area experiences high electric field strength.* 2

3.1 *1D geometry and 2D geometry with two air wedge. The 1D geometry is derived as a cut line through the 2D model as shown in (b).* 14
3.2 *The 2D geometry with one air wedge and the scaled down 2D geometry.* 14
3.3 *Plot of tabulated values for the Townsend's first ionization coefficient as a function of reduced electric field. The y-axis is on logarithmic scale.* 17
3.4 *Plot of tabulated values for the reduced attachment coefficients as a function of reduced electric field. The x-axis and y-axis are on logarithmic scales.* 17
3.5 *Plot of tabulated values for electron drift velocity as a function of reduced electric field. The x-axis and y-axis are on logarithmic scales.* 18
3.6 *Plot of tabulated values for the characteristic electron energy as a function of reduced electric field. The x-axis is on logarithmic scales.* . 19
3.7 *Standard lightning impulse with front time* $1.2\,\mu s$ *and* $50\,\mu s$ *time to half-value. The peak value is set as 1 and the duration is* $100\,\mu s$ . . . 20
3.8 *Consecutive lightning impulses with different durations respectively.* . 21
3.9 *Mesh setting for the overall computational domain and the critical region. Smaller size elements are assigned to the critical region where charging behaviours are expected.* 22

4.1 *Labeling of 1D simulation model geometry. Two air domains and four interfaces between air and insulators are marked.* 26
4.2 *Capacitive current densities at the ground side for* $+75\,kV, +80\,kV, +100\,kV$ *and* $+120\,kV$*. Discharge initiate at around* $+80\,kV$*.* 26
4.3 *Electric field strength and positive ions concentration in log scale under the lightning impulse voltage of* $+100\,kV$*. Localized discharge in domain 1 can be observed.* 27
4.4 *Electric field strength and positive ions concentration in log scale under the voltage of* $+120\,kV$*. Discharges emerge in both domain 1 and domain 2.* 29
4.5 *Positive surface charge accumulation in log scale on boundary 2 and boundary 4 under the voltage of* $+100\,kV$ *and* $+120\,kV$*. Positive ions produced by discharges will be accumulated on boundary 2 and 4.* 30

4.6 *Negative surface charge on boundary 1 and positive surface charge on boundary 2 in log scale under the voltage of* $+100\,\mathrm{kV}$*. Negative surface charges start increasing earlier due to the high electrical mobility of electrons.* 31
4.7 *Electron concentration in log scale in domain 2 for* $ad_p = 0.1$ *and* $ad_p = 0.5$ *under* $+160\,\mathrm{kV}$*. The high concentration gradient will lead to un-physical results which can be improved with artificial diffusion added.* 32
4.8 *Capacitive current densities at the ground side for tuning parameters of* $0.1, 0.5$ *and* 0.9 *under* $+160\,\mathrm{kV}$*. Results will be distorted given tuning parameters too high.* 33
4.9 *Rounded triple junction geometry used and triple junction in test set up. The rounded corner conforms more with the set up.* 34
4.10 *Capacitive current for* $+80\,\mathrm{kV}$ *and* $+120\,\mathrm{kV}$ *lightning impulse voltage with the gel height of* $3\,\mathrm{mm}$*. Higher voltage level will cause more intensive discharges.* 35
4.11 *Negative surface charges on vertical boundary in log scale under lightning impulse voltage of* $+120\,\mathrm{kV}$ *with the gel height of* $3\,\mathrm{mm}$*. Accumulation occurs after the discharges.* 35
4.12 *Electric field strength for four time instants under* $+120\,\mathrm{kV}$ *with* $3\,\mathrm{mm}$ *gel height. Discharge emerges in region around triple junction and high field region obtained along vertical boundary.* 36
4.13 *Positive ions concentration in log scale for four time instants under* $+120\,\mathrm{kV}$ *with* $3\,\mathrm{mm}$ *gel height. Positive ions are generated by discharges and drifted in the direction of the electric field.* 37
4.14 *Positive ions concentration after discharge under impulse voltage of* $+80\,\mathrm{kV}$ *with* $3\,\mathrm{mm}$ *gel height. Discharge restricted in lower region.* . . . 38
4.15 *Negative surface charge on vertical boundary in log scale under* $+80\,\mathrm{kV}$ *with* $3\,\mathrm{mm}$ *gel height. Lower concentration negative charge on stress cone surface for* $+80\,\mathrm{kV}$*.* 38
4.16 *Rounded edge 2D model geometries with gel height of* $3\,\mathrm{mm}$ *and* $5\,\mathrm{mm}$*. Higher gel surface will stress the air around triple junction more.* . . . 39
4.17 *Capacitive current and negative surface charge in log scale for* $3\,\mathrm{mm}$ *and* $5\,\mathrm{mm}$ *gel heights under*$+80\,\mathrm{kV}$ *LI. Higher gel surface will intensify the discharges.* 40
4.18 *Capacitive current for voltage of* $-120\,\mathrm{kV}$ *with* $3\,\mathrm{mm}$ *gel height. Discharge occurs at around* $0.41\,\mu\mathrm{s}$*.* 41
4.19 *Electric field strength in four time instants for* $-120\,\mathrm{kV}$ *with* $3\,\mathrm{mm}$ *gel height. Gel will be stressed with high electric field strength compared with positive case.* 42
4.20 *Positive ion concentration in log scale at four time instants for* $-120\,\mathrm{kV}$ *with* $3\,\mathrm{mm}$ *gel height. Discharge develops along the gel for negative polarity voltage.* 43
4.21 *Scaled-down geometry with smaller size and a deeper* $8\,\mathrm{mm}$ *wedge.* . . 45
4.22 *Capacitive current under the voltage of* $+65\,\mathrm{kV}$*.* 46

4.23 *Electric field strength in four time instants after the discharge under* +65 kV. *Superimposed field direction reversed after* 10 µs *which will change the drift motion of free charge carriers.* 47
4.24 *Negative surface charge on stress cone and gel boundary until* 100 µs *under* +65 kV. *Negative surface charges on lower part of boundary first increase and then decrease due to field reversal.* 48
4.25 *Negative surface charges concentration on stress cone and gel boundary at the same time instant for three* +65 kV *impulses respectively. Higher amount of surface charge obtained with more impulses applied. The rate of increase is different for different part on the boundaries.* . 49
4.26 *Negative surface charge on curved gel surface at the same time instant of* 0.45 µs *and capacitive current for the second and third impulse. Discharge will be intensified with more impulses applied.* 50
4.27 *Electric field strength at the same time instant of* 0.45 µs *for the second and third impulse. The electric field strength is enhanced by the surface charge for the third impulse, resulting in more intensive discharges.* 50
4.28 *Capacitive current and surface charge concentration at the same time instant* 4500 µs *for three impulses.* 51
4.29 *Surface charge on stress cone and gel boundary until* 0.4 s. 53
4.30 *Capacitive currents for cases with* 4500 µs *and* 0.4 s *surface charges as initial values. Surface charges for* 4500 µs *and* 0.4 s. 53
4.31 *Capacitive current and surface charge concentration at the same time instants for three* +65 kV *impulses with gel height of* 4 mm. *The accumulated surface charge will intensify the discharges in later impulses.* 54
4.32 *Electric field distribution around critical region at the same time instant (*0.2 µs*) for negative and positive polarity secondary impulse before the discharge. Higher electric field strength obtained for negative secondary impulse.* 54

List of Tables

3.1 *Material properties assigned to the computational domains* 15

A.1 Geometry parameters used in the simulation model I
A.2 Constant parameters used in the simulation model II
A.3 Variables used in the simulation model II

1
Introduction

Corona discharges emerge in the gaseous medium exposed to intense electric field. They are utilized in many areas, such as air filtration and ozone generation. However, for electrical power transmission system and high voltage equipments, corona discharges are encumbrances and may result in power losses and insulation faults. The aim of this thesis is to simulate and analyze the charging behaviour along the air-polymer surface inside a cable termination during the corona discharge. In this introduction chapter, the background, aim, problem, scope and sustainability aspects of the thesis work are provided.

1.1 Background

Previous works have been carried out to study how the charges can accumulate along dielectric surfaces and distort local electric field distributions. Such phenomenon might lead to surface flashover faults under extreme conditions which threats the gas-solid insulation in high voltage equipments. Atmospheric lightning can cause external overvoltage for electrical energy system resulting in extreme high dielectric strength. However, not too much studies have been carried out on the subject on charges accumulation under multiple lightning impulses. Thus it's necessary to investigate relevant charging behaviours and their impact under lightning impulse voltage.

NKT HV Cables AB has proposed a unique patented prefabricated dry type HVAC cable termination in 2012. The filling compound between stress cone and housing insulator is gel which will be pressurized and formed a curved surface when the cable is plugged in during installation. Static calculations on the electric field have been carried out as shown in Fig.1.1. The triple junction formed by air, gel and stress cone will experience high tangential field and is the critical region where discharges initiate.

Certain flashover and punctuation can be observed in the termination under impulse voltage testing at elevated voltages. The lightning impulse testing usually composites of multiple impulse voltages with 30 s to 60 s between surges and distinct magnitudes and polarities. Hypothesis has been made that the surface charge accumulation during consecutive impulses will intensify the field strength around critical region with more surges applied. Thus dynamic simulations of surface charging process along the critical region are highly desirable for better understanding of the

charging behavior and cause of failure under standard impulse voltages.

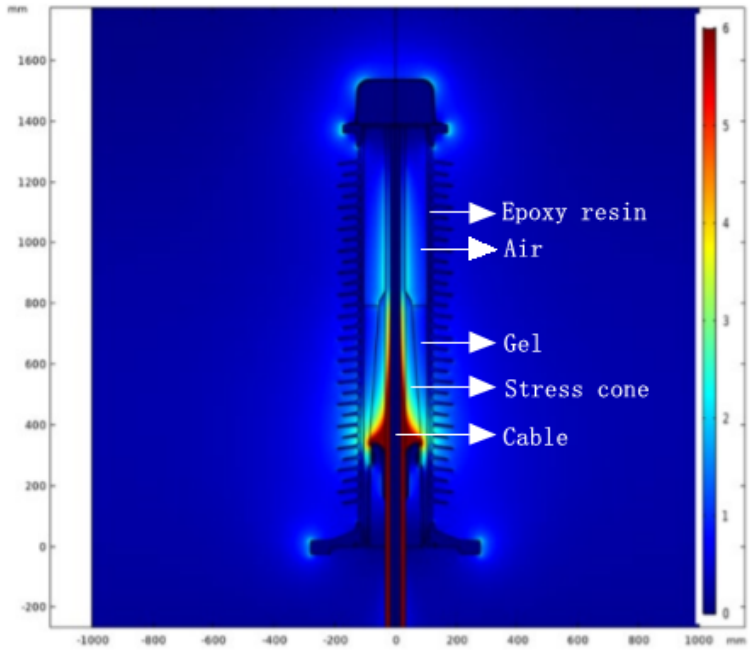

Figure 1.1: *Static calculation of electric field strength inside the cable termination. The triple junction area experiences high electric field strength.*

In a previous work, Georgii Karman has developed a FEM-model to analyze experiments of corona from wire in free air under high frequency triangular voltages [1]. Martin Macken carried on the study with the focus of simulation under lower frequencies voltage with and without a cylindrical insulator [2]. The present thesis can be treated as a continuation of their works but based on a different gas-solid insulation composition under standard lightning impulse voltage and voltage series. A related experimental work is conducted by Philip Hoang at the same time to inspect the charge distribution and movement on air-epoxy interface.

1.2 Aim

The aim of this thesis work is to inspect the corona based on the relevant HVAC termination design at the standard lightning impulse. How the discharge develops will be inspected and the influence of different geometry parameters and voltage polarity and levels on the electric field will also be studied. Charge accumulation along the polymer surface under lightning impulse is of interest and their impacts on the electric field and discharges under consecutive impulses is one main topic of this thesis work.

1.3 Problem

The first problem in the numerical modeling is the great demand of computational power and time, especially when several lighting impulses are applied. Such obsta-

cle can be eliminated by adjusting the time steps for different time range or using specific finer mesh setting in computational area of interest. Nevertheless, certain balanced should be reached to meet the accuracy requirement.

Another problem in the simulation is the convergent problem caused by sharp edges in geometry. The triple junction will turn into a sharp edge in the model which causes convergent problem for the simulation. It is of utmost importance to implement a well defined geometry that the sharp edge is smoothed while can describe the test setup correctly.

1.4 Scope

Certain assumptions and trade-offs have been made in the model to simplify the simulation while ensuring the results are realistic.

- The surface charges accumulated on the polymer surface are assumed to be sedentary that the charge trapping-detrapping and surface conduction physics are not included in the boundary condition. This reduces the complexity of implemented physics and possible unphysical behaviours in the results.
- The empirical data used in the model is from Martin's previous work [2] that has been adjusted and validated the specific experimental work. It is assumed the same data is also applicable in the model of this thesis work.
- The mesh setting is rather coarse in the region of less interest to save the computational power and time. Simulation time steps are also adjusted for different time range that rather small time steps are assigned when the discharges emerge.

1.5 Sustainability and ethical aspects

The cable terminations are usually divided based on the insulating media used in the system. The dry-type cable termination, as studied in this study, is environmental advantageous compared with gas-filled and oil-filled. Compared with gas-filled termination, it avoids the use of SF_6 which has great greenhouse effect and reduce the potential of oil leakage during installation and operation compared with oil-filled. The dry-type is also preferable since there is less risk of secondary damage to the society in case of an internal arc which may lead to an explosion. The cable termination studied in this work is prefabricated and requires less manpower to install.

However, the dry-type terminations are usually much expensive than the gas-filled and oil-filled terminations for highest voltage level. And the cable termination discussed in this study is for HVAC transmission which compared with HVDC has higher power losses and environmental impacts.

As for the simulation model, since it's based on previous work [2], contents and values adapted from have been clearly stated. Related product details have been obtained from NKT HV Cables AB under permission.

2

Fundamental physical processes in gas discharges

Gas discharges can be divided into breakdowns or flashovers that forming a conductive channel and partial discharges that do not directly lead to breakdowns. Under uniform or weakly non-uniform field, if the initiation condition is met, a breakdown of voltage happens immediately [3]. However, if the field distribution is strongly non-uniform, the ignition condition can be reached in a small and highly stressed volume where the discharge can not propagate along the whole distance that leads to a entire breakdown [4]. Such partial discharges are usually referred to corona discharge. In this chapter, the physical process and underlying theory of the corona discharge is given.

2.1 Generation and losses of charge carriers

Under standard atmospheric and low field condition, an initial conductivity of $2.5 \times 10^{-14} S/m$ to $5.0 \times 10^{-14} S/m$ can be observed resulting from the free charges in the gas due to radiation or thermal ionization. Such background ionization generates electron-ion pairs carrying elementary charge of $q = 1.6 \times 10^{-19} C$ and can be characterised with a rate R_0.

If an electric field $\mathbf{E}$ is applied, the electrostatic force $\mathbf{F}$ will be added on the charged particles according to Coulomb's law

$$\mathbf{F} = \mathbf{E}q \tag{2.1}$$

The ions and electrons will be drifted by the force with a velocity of

$$\mathbf{w} = \mathbf{E}\mu \tag{2.2}$$

where μ is the mobility of the charged particle. Particles will gain higher velocity under increased field strength which means higher energies Q can be collected as

$$\mathbf{Q} = \mathbf{E}q\lambda \tag{2.3}$$

where λ is the free path of the particle travels. Electrons play important roles in electrical discharge in gas. Through inelastic collisions with other molecules, the electron kinetic energy grows until the energy exceeds the ionization energy

of molecule. In this case, the ionization caused by electronic collision produces additional electrons which are accelerated in the electric field and lead to more ionization collisions. The symbolic equation describing the reaction is shown as

$$e^- + A \rightarrow e^- + e^- + A^+ \tag{2.4}$$

where A, A^+, e indicate molecule, positive ion and electron. There are different mechanisms for atoms to absorb energy and the effects produced is the same: excitation and ionization of atoms. Typical processes include ionization by ionic collision, photo-ionization and thermal ionization[5] which will not be further discussed. A generic rate describing all of the ionization reaction is defined as

$$R_{ion} = \alpha n_e w_e \tag{2.5}$$

where α is Townsend's first ionization coefficient, n_e is the density of electrons and w_e is the drift velocity of electrons.

The negative ions in gas constitute a source of free electrons. Electrons detach from the negative ions in the presence of high electric field[6]. The reaction is illustrated as

$$A^- + B \rightarrow e^- + AB \tag{2.6}$$

The rate of detachment can be described by a detachment coefficient k_{det} is, density of negative ions n_n and density of gas N.

$$R_{det} = k_{det} n_n N \tag{2.7}$$

In electronegative gases, electrons can attach to the neutral gas molecules with a high degree of electron affinity [7]. Stable negative ions are therefore generated. The predominant dissociative attachment is stated according to the equation below

$$e^- + AB \rightarrow A^- + B \tag{2.8}$$

The attachment process can be characterised with a attachment rate

$$R_{att} = \eta n_e w_e \tag{2.9}$$

where η is the attachment coefficient describing the generic process.

A recombination process is the process where charged particles recombine to form neutral species. Electron can recombine with positive ion, resulting in two neutral particles

$$e^- + AB^+ \rightarrow A + B \tag{2.10}$$

However, such direct recombination between electron and ion is not frequent because of the high energy of electron. Ion-ion recombination involves positive and negative ions occur as two-body or three-body collisions as shown below.

$$A^- + B^+ \rightarrow A + B \tag{2.11}$$

$$A^- + B^+ + C \rightarrow A + B + C \tag{2.12}$$

It is to be noted there are more different reactions of ion-ion collisions that the equations above are just used to illustrate the basic of the process. Different rates can thus be defined to describe the recombination reactions.

$$R_{rec}^{ei} = \beta_{ei} n_e n_p \tag{2.13}$$

$$R_{rec}^{ii} = \beta_{ii} n_n n_p \tag{2.14}$$

where β_{ei} is the electron-ion recombination coefficient, β_{ii} is the ion-ion recombination coefficient and n_n, n_p and n_e are the concentrations of negative ions, positive ions and electrons respectively [8].

2.2 Transport of charged species due to drift and diffusion

The movements of ions and electrons caused by drift and diffusion constitute the total flux in discharge plasma [9]. As shown in equation 2.1 and 2.2, the swarm of electrons or ions subjected to a electric field will hold a drift velocity of $\mathbf{w}$. The mobility μ is dependent on the atmospheric conditions which after correction is used to calculate the flux due to the applied field

$$\Gamma_{drift} = \mathbf{E} \mu_i n_i \tag{2.15}$$

However, the result of diffusion process is a tendency of keeping the concentration of ions the same in the whole gas volume. The gradient of ion concentration will be subjected and the ions will move from the high concentration parts to the low concentration parts. The redistribution of ions can be illustrated as recombination effect in high concentration region and ionization effect in low concentration region [5]. The diffusion flux can be calculated as

$$\Gamma_{diff} = -D_i \nabla n_i \tag{2.16}$$

where D_i is the diffusion coefficient and ∇n_i is the concentration gradient. The Einstein's relation describes the relationship between D_i and mobility μ_i of the same single charge

$$D_i = \mu_i \frac{k T_i}{q} \tag{2.17}$$

where k and T_i stand for Boltzmann's constant and ionic temperature.

2.3 Hydrodynamic description of charge motion

The dynamic of charge carriers in discharge plasma can be described by continuity equations if all the quantities are considered conserved in a closed system. Three partial differential equations can be formulated for electrons, positive ions and negative ions respectively by Smoluchowski equation

$$\frac{\partial n_e}{\partial t} + \nabla \cdot (-n_e \mathbf{w_e} - D \nabla n_e) = R_e \tag{2.18}$$

$$\frac{\partial n_n}{\partial t} + \nabla \cdot (-n_n \mathbf{w_n} - D\nabla n_n) = R_n \tag{2.19}$$

$$\frac{\partial n_p}{\partial t} + \nabla \cdot (n_p \mathbf{w_p} - D\nabla n_p) = R_p \tag{2.20}$$

Where n is the concentration of charge carriers, D is the diffusion coefficient, **w** is the drift velocity and R is the source term representing the total rate of generation and loss of species. It is noted that the drift velocities for negative ions and electrons have negative sign in equation 2.21 and 2.22 that indicating a opposite drifting direction against the field. The source terms for each charge carriers can be implemented below based on the physical process described in chapter 2.1 .

$$R_e = R_0 + R_{ion} + R_{det} - R_{rec}^{ei} - R_{att} \tag{2.21}$$

$$R_n = R_{att} - R_{det} - R_{rec}^{ii} \tag{2.22}$$

$$R_p = R_0 + R_i on - R_{rec}^{ei} - R_{rec}^{ii} \tag{2.23}$$

2.4 Space charges and surface charges accumulation on interfaces

When the charge carriers move close to the dielectric surface, it is assumed that the ions and electrons trapped immediately on the perfectly absorbing surface and only charges are left at the surface [10]. Surface charge density is defined as

$$\sigma = \frac{q}{A} \tag{2.24}$$

where q is the amount of charge on a specific area A. The rate of surface charge density is related to the fluxes entering the surface

$$\frac{\partial \sigma}{\partial t} = q(\mid \Gamma_p \mid - \mid \Gamma_n \mid - \mid \Gamma_e \mid) \tag{2.25}$$

where Γ indicate the fluxes of each charge carriers. It is noted that the negative ion and electron fluxes are subtracted which also correspond to their opposite movement to the field.

Due to the high electrical mobility, electrons will travel much faster in the air and reach the dielectric surface first. The remaining space charges affects the field distribution and alters the corona development. The space charge density ρ in the air volume is defined as

$$\rho = q(n_p - n_n - n_e) \tag{2.26}$$

where n_p, n_n and n_e are the concentrations of positive ions, negative ions and electrons. The electric field **E** is defined as the gradient of electrical potential ϕ

$$\mathbf{E} = -\nabla\phi \tag{2.27}$$

Through Maxwell's first equation

$$\rho = \nabla\varepsilon\mathbf{E} \tag{2.28}$$

the Poisson's equation used for calculating electric field strength can be obtained as

$$-\nabla(\varepsilon_0\varepsilon_r\nabla\phi) = \rho \tag{2.29}$$

where $\varepsilon_0, \varepsilon_r$ and ε stands for the permittivity of free space, relative permittivity and dielectric respectively. ρ is the density of charges contained in the discharge region which constitute of both space charges and surface charges.

The space charges alter the electric field in different ways under different polarities. A point to plane arrangement which have non-uniform field distribution can be used as an example. Under positive polarity voltage, the avalanche develops in the direction of increasing field strength towards anode. The electrons are quickly absorbed by the positive point electrode and positive ions are remained in space. Thus the electric field is reduced in front of the point electrode while increased in front of the space charge. During streamer discharge, the ionization activities extend to the low-field region in the form of corona globules. Such propagation is supported by the electric field generated by the positive space charges. However under negative polarity, electrons are repelled from the cathode and attach to molecules forming negative space charges in the low field region. The positive space charges form a charge cloud around the point electrode. The field around the cathode is enhanced while reduced in the ionization region. The onset and breakdown voltage thus deviate for different polarities and is known as 'polarity effect'[3].

2.5 Main stages of discharge development

As stated in previous chapter, collision ionization will produce additional electrons which will also be accelerated and generate more electrons resulting in an electron avalanche. The number of electrons generated over a distance d in a homogeneous field can be calculated as

$$n_e = n_0 \exp(\alpha d) \tag{2.30}$$

where n_0 is the number of initial electrons and α is Townsend's first ionization coefficient. The Townsend's first ionization coefficient α is the number of electrons generated by a single electron through collision ionization per unit length. It is expected that α is dependent on the energy gained through the free path. Besides, at a constant temperature the free path λ is inversely proportional to pressure p which is proportional to gas density N. As shown below

$$\frac{\alpha}{N} = f(\frac{E}{N}) \tag{2.31}$$

the ionization coefficient α is dependent on reduced field strength $\frac{E}{N}$.

The generated ions will interact with cathode and emit photons which can generate electrons by photoionization. The new electrons will then trigger new avalanches.

This is called the secondary ionization process or feedback process. The total number of electrons reaching anode can be termed as

$$n_t = \frac{n_0 e^{\alpha d}}{1 - \gamma(e^{\alpha d} - 1)} \tag{2.32}$$

where γ is the second ionization coefficient. If the equation is singular which indicates finite number of charges, then the discharge is sustained[11]. On the contrary, if the convergence condition is not met, the initial electrons will be infinite. Conductive channel between electrodes will be formed and the direct breakdown will emerge in uniform field. Thus the ignition condition for Townsend mechanism can be described as

$$1 - \gamma(e^{\alpha d} - 1) \leq 0 \tag{2.33}$$

which can be explained that for the single initial electron at least one new electron needs to be generated by avalanche growth or feedback process to trigger consecutive avalanches[12]. The Paschen's law describes the breakdown voltage in uniform field.

$$V_{bd} = \frac{B \cdot pd}{\ln \frac{A \cdot pd}{\ln 1 + 1/\gamma}} \tag{2.34}$$

where A and B is characteristic constants for gases, p is the gas pressure and d is the inter-electrode spacing. The breakdown voltage or inception voltage under uniform field is a function of the product pd [3].

In an non-uniform field, the electric field will be greatly influenced by the space charge if the avalanche grows to certain level [13]. The relative immobile positive space charges will remain in the avalanche tail and the electrons will form a negative spherical avalanche head which will result in a field-enhancement at the front of the avalanche head. This will intensify the ionization collision and photoionization process and provide initial electrons for following avalanches. A conductive path will be generated quickly with all the avalanches being super-positioned swiftly which is called a streamer discharge.

2.6 Discharge current

The discharge current collected at the electrodes during corona discharge can be divided into ionic component and displacement component.

$$I_{tot}(t) = I_{ion}(t) + I_{disp}(t) \tag{2.35}$$

The ionic current component depends on the conduction of moving charges and displacement component relate to the time varying field. Both components can be illustrated as

$$I_{ion} = AJ_{ion} = qA\mathbf{E}(n_p\mu_p - n_n\mu_n - n_e\mu_e) \tag{2.36}$$

$$I_{disp} = AJ_{disp} = A\frac{\partial \mathbf{D}}{\partial t} = A(\varepsilon\frac{\partial \mathbf{E}}{\partial t}) \tag{2.37}$$

where J represents the corresponding density and A is the area of the electrodes. The displacement current constitute of two parts: first related to geometrical capacitance of the system and second part due to the space charges influences on the electric field dynamics. The first part can be calculated as

$$I_{cap0} = C\frac{\partial U}{\partial t} \tag{2.38}$$

where U is the voltage applied and C is the responding capacitance. It is noted that since no major conduction of charges appears in dielectric materials, the displacement current especially the second part is a good indication of discharges in the system.

3

The model and computer implementation

In this chapter, the step by step description of implementation of the problem in COMSOL Multiphysics is provided. The geometries and materials are first illustrated and followed by depiction implementation of multi-physics. The ways of how the parameters and variables are defined, how the finite element meshing is set, how the stabilization method is implemented and how the current calculations are performed will be explained.

It is to be noted since the 1D model used is expanded from previous work [2], the main focus of this chapter will be on the implementation in 2D model. Readers can get more information about 1D model implementation from [1] and [2]. The principle and physics included are the same while changes have been made on the geometry and relative boundary conditions.

3.1 Geometry and materials

Since two different models are used, the geometries and materials for 1D and 2D model are introduced separately. The 1D plane geometry is a coaxial geometry defined as a cut line through a 2D geometry as shown in Fig.3.1. The computational domain represents a 1D simplification of the region around the gel surface starting at the inside of the stress cone where voltage is applied, to the air gap between stress cone and gel, gel and then to the grounded insulator surface. The distance between potential and ground in the used 1D geometry is 80 mm.

The leftmost point represent the stress cone surface where and the rightmost point is the grounded insulator surface. An interval is defined to represent the total length and four points are used to represent the interface between different materials. The points from left to right indicate interface between air and stress cone, two interfaces between air and gel and interface between air and insulator.

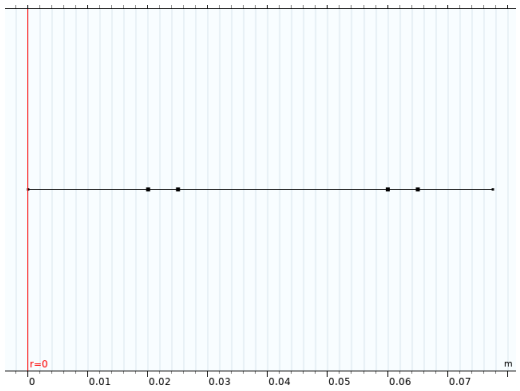

(a) *1D geometry.*

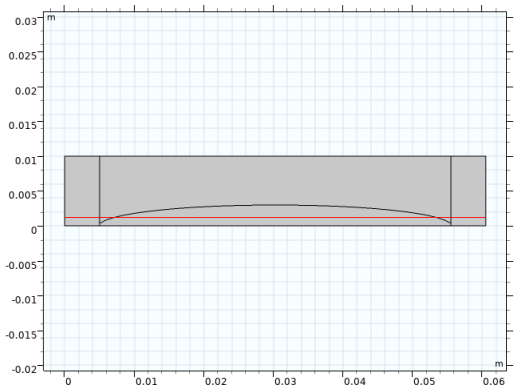

(b) *Two air wedge 2D geometry.*

Figure 3.1: *1D geometry and 2D geometry with two air wedge. The 1D geometry is derived as a cut line through the 2D model as shown in (b).*

In this study 2D Cartesian models are used only considering the air gap between the stress cone and gel compared with 1D geometry in order to reduce the complexity of the model. As shown in Fig.3.2a, four areas are used to represent the components. The gel bump in between is built by a quarter of ellipse and a rectangle. The connected gel, stress cone and air will form a sharp triple junction bringing difficulties on mesh setting and convergence of solutions. Thus, a fillet node is used to smooth up the triple junction and create a circular rounded corner. A line and a *Mesh Control Edges* node are added for setting the meshing element in later section. The distance between the potential and the ground in this 2D geometry is 60 mm. Besides, a scaled-down 2D geometry as shown in Fig.3.2b is used to reduce the computational power and time demand and will be explained further in later chapters. In this geometry the distance between potential to ground is reduced to 30 mm. The steps of the implementation is the same with different parameters used. All the geometry parameters are included in Table A.1 in appendix.

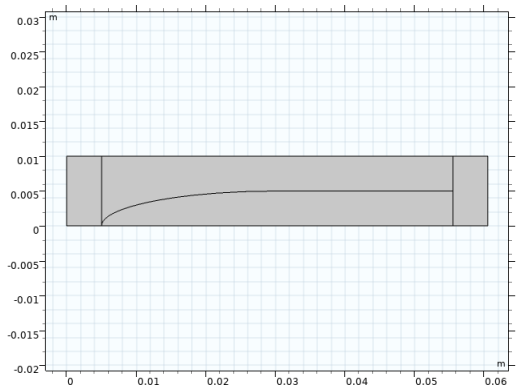

(a) *One air wedge 2D geometry.*

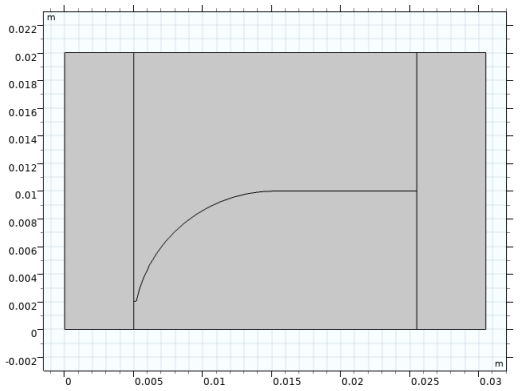

(b) *Scaled down 2D geometry.*

Figure 3.2: *The 2D geometry with one air wedge and the scaled down 2D geometry.*

It is to be noted that the parameters for 1D model are not related to 2D models since the 1D model is expended from the previous work [2] and is used to assure

the feasibility of implemented physics under lightning impulses and is also useful for basic understanding of the charging dynamics. Thus the term 'cut line' used is more of an expression for describing the geometry than a real cut line.

Four materials are created and assigned to each domain under the *Material* node, where the relative permittivities are defined as shown in Table.3.1 for calculating electric field.

Table 3.1: *Material properties assigned to the computational domains*

Material	Relative permittivity ε_r
Air	1.0
Stress cone	3.0
Gel	3.5
Epoxy insulator	5.7

3.2 Multiphysics aspects

3.2.1 Poisson's equation and calculations of the electric field

The *Electrostatics* physics interface in AC/DC model is included for computing the electric field strength through Poisson's equation 2.29 introduced in previous chapter. Several nodes are included by default. The *Charge Conservation* sub-node implements charge conservation equations for electric displacement field according to Gauss' law for all the domain. It accounts for the left hand side of Poisson's equation. The relative permittivity is set *from material* that has already been introduced in last section. The *Initial Values* sub-node adds an initial electric potential to the domains as an initial guess for the non-linear solver. Since charge carriers exist in the air, the *Space Charge Density* sub-node is used to add a space charge density variable rho only to the air domain. An *Electric Potential* sub-node is added to assign the voltage input to the stress cone far-side surface as boundary condition and a *Ground* sub-node is assigned to the insulator far-side interface as well. The *Surface Charge Density* sub-node provides surface charge boundary condition of

$$\mathbf{n}(\mathbf{D_1} - \mathbf{D_2}) = \rho_S \tag{3.1}$$

where ρ_s is the surface charge density accumulated which in the study is defined by variable $sigma1$. The domain is assigned to the boundaries between air and stress cone, gel and insulator since the surface charges are considered as transformed from the space charges. The rest of the boundaries are assumed to be no charge under *Zero Charge* sub-node. Combined with the space charge, the right hand side of Poisson's equation is determined. The charge transport and accumulation is described in next section.

3.2.2 Charge transport equations

The *Transport of Diluted Species* interface is used to model transport of duplicated species by convection and diffusion in chemical system. The dependent variable is

the mole concentration that e for electrons, *pos* for positive ions and *neg* for negative ions and one physics node is assigned for each charge carriers. Since the the drift and diffusion only take place in air domain and no charge transport is expected with insulating materials, only the air domain is applied with these physics.

Consistent and inconsistent stabilization methods are available for numerical stabilization. In consistent method, streamline diffusion and crosswind diffusion is available while the isotropic diffusion is accessible for inconsistent method. The isotropic diffusion stabilization is chosen to reduce the oscillations in the solution and avoid non-physical negative concentration magnitude ascribed to steep derivatives of charge densities. A tuning parameter ad_p is given to add the artificial diffusion. Detailed description will be provided in later chapter.

In the *Transport Properties* sub-node, the left hand side of equations 2.18-2.20 are determined. The charge carriers drift velocity $\mathbf{u}$ is determined by corresponding mobility mu_n, mu_p and mu_e and also electric field strength while the diffusion coefficients are defined as the variables D_n, D_p and D_e. The *Initial Values* sub-node is used to apply initial concentration to each charge carriers in the air domain with $n0$ for positive ions and negative ions and $1\,\mathrm{mol/m^3}$. The sub-node *Reactions* is used to define the consumption and production of the specific species with variables $source_e, source_n$ and $source_p$ implemented as reaction rate which governs the right hand side of equations 2.18-2.20.

An *Outflow* sub-node is included to describe the outflow of charge carriers assuming zero diffusion at the outlet boundaries and convection is the dominating process

$$\mathbf{n}(-D\nabla c) = 0 \tag{3.2}$$

The sub-node is assigned for all the boundaries where space charges will transfer into surface charges in order to avoid the charges being double accounted for.

3.2.3 Surface charges accumulation

The *Boundary ODEs and DAEs* node under *Equation-Based modeling* is used to build up the partial differential equations for all the charge carriers. The default equations for *Distributed ODEs* sub-node is shown below

$$e_a \frac{\partial^2 u}{\partial t^2} + d_a \frac{\partial u}{\partial t} = f \tag{3.3}$$

where e_a, d_a and f is the mass coefficient, damping coefficient and source term. In our case, e_a and d_a is chosen as 0 and 1 respectively and u is the surface charge $sigma1$. The source term is defined as

$$f = q(\mid \Gamma_p \mid - \mid \Gamma_n \mid - \mid \Gamma_e \mid) \tag{3.4}$$

the equation 2.25 accounting for surface charge accumulation is described. When the charge carriers move to the interfaces between air and stress cone, gel and insulator, the *Outflow* sub-node remove them from the air domain and the ODEs account them as surface charge. The resulted values are then used as surface charge input for Poisson's equation described before.

3.3 Model coefficients, parameters and variables

In this section the coefficients, parameters and variables defined and used in this study are explained. It is noted that since the work is based on the studies in [2], the values chosen have been proven feasible under the corresponding test set up. The majority of the values are kept the same and no extra fitting and validation of values are made in this study due to the lack of experimental results at the start of the work.

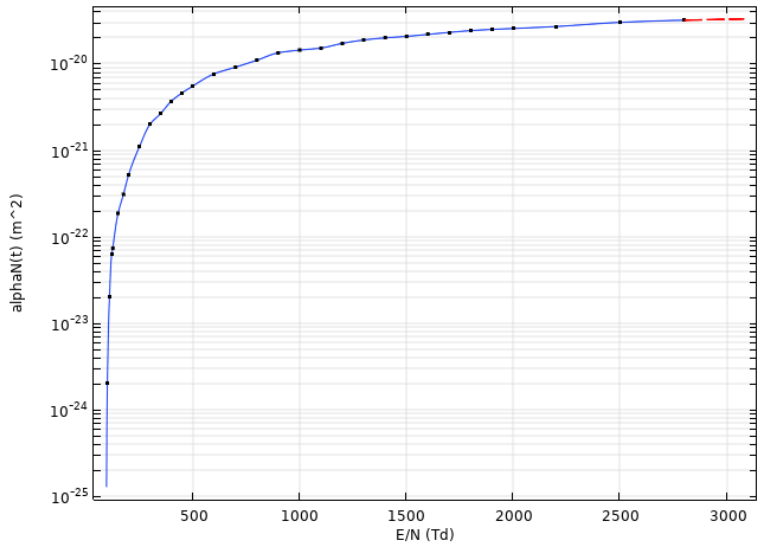

Figure 3.3: *Plot of tabulated values for the Townsend's first ionization coefficient as a function of reduced electric field. The y-axis is on logarithmic scale.*

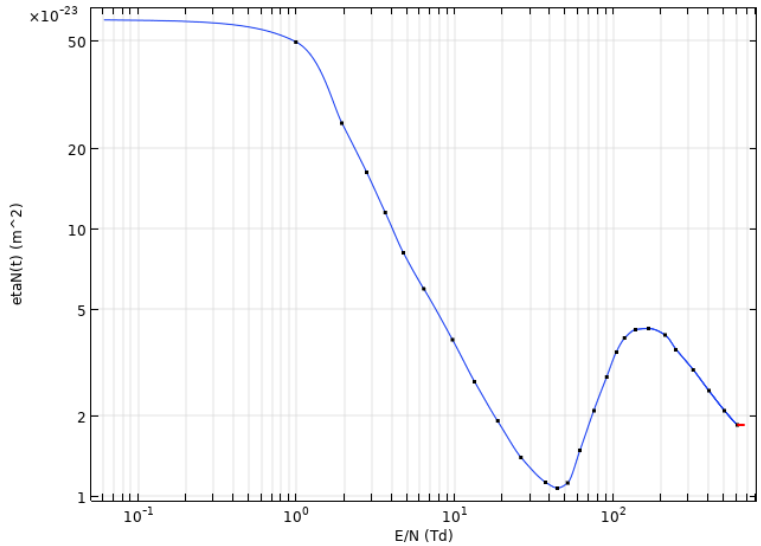

Figure 3.4: *Plot of tabulated values for the reduced attachment coefficients as a function of reduced electric field. The x-axis and y-axis are on logarithmic scales.*

The *Interpolation Function* under *Global Definitions* node is used to implement the input tabulated data. All the tabulated data source from [2] and has been fitted and verified under related experimental results. The reduced ionization coefficient $\frac{\alpha}{N}$ is applied to calculate the ionization coefficient R_ion discussed in chapter 2. The tabulated values of $\frac{\alpha}{N}$ from [14] are used in this study and shown in Fig.3.3. The reduced attachment coefficient $\frac{\eta}{N}$ for calculating attachment rate R_{att} is implemented in similar manner with the tabulated data from [15]. The relationship between reduced attachment coefficient $\frac{\eta}{N}$ and electric field is shown in Fig.3.4. It is noted that the value is rather high for low electric field which attributes to the dominating three body attachment process.

The electrons drift velocity w_e is electric field dependent and the relationship with reduced electric field $\frac{E}{N}$ is also settled by tabulated data from [14] and shown in Fig.3.5 Besides, the diffusion coefficient for electrons are calculated by the electron characteristic energy $\frac{D}{N}$ which is treated as a function of reduced electric field in Fig.3.6.

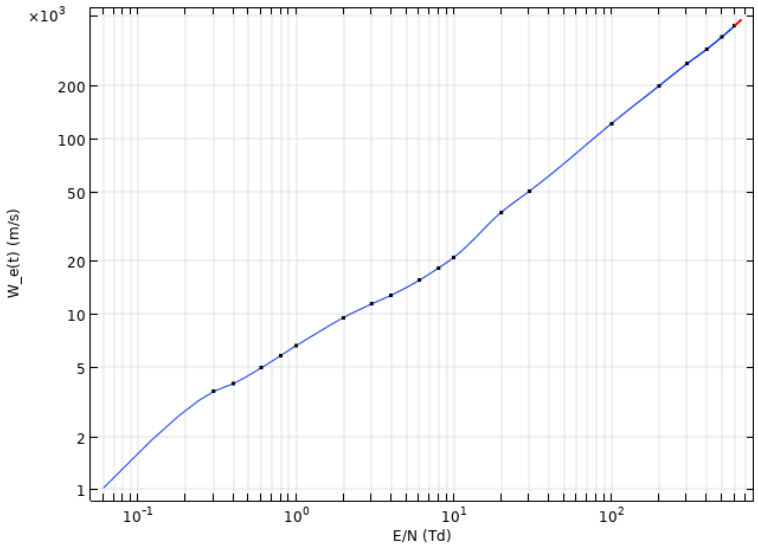

Figure 3.5: *Plot of tabulated values for electron drift velocity as a function of reduced electric field. The x-axis and y-axis are on logarithmic scales.*

The *Parameters* sub-node under the node *Global Definitions* is used to define constant values used throughout the entire model. A geometry *Parameters* sub-node is defined to store the values used to build the relative geometry as discussed in section 3.1. Another sub-node is built to declare other parameters used in the model and the table is shown as Table A.2 in the Appendix.

The background ionization rate, secondary emission coefficient, electron-ion recombination coefficient and initial ion concentration discussed in chapter 2 are defined as $R0, gamma, beta_{ei}$ and $n0$. The mass of electrons and negative oxygen ions O_2^- is set as m_e and m_n with the mass of positive oxygen ion m_p and molecule m_g calculated accordingly. The mobility of positive and negative ions are less field dependent and

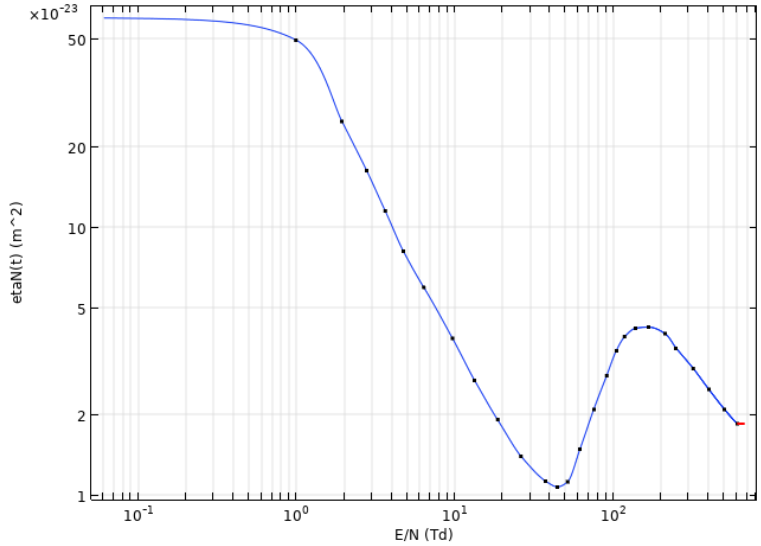

Figure 3.6: *Plot of tabulated values for the characteristic electron energy as a function of reduced electric field. The x-axis is on logarithmic scales.*

set as constant value mu_p and mu_n. The actual pressure and temperature, pg and Tg are not the main focus of the study and thus kept the same as reference values $p0$ and $T0$. The voltage amplitude V_amp are set as 80 kV initially and the tuning parameter ad_p mentioned in section 3.2.2 is set as 0.5 initially.

A *Variables* sub-node under *Global Definitions* node is set to define the expression being used through the whole study. The implemented variables can be found in Table A.3 in Appendix. As described in equation 2.17, the diffusion coefficients D_p and D_n for positive and negative ions are calculated while the coefficient for electrons D_e is defined as the product of characteristic electron energy and mobility of electrons. The space charge density rho is calculated from equation 2.26 and the source terms R_e, R_n and R_p for charge carriers are calculate from equations 2.21, 2.22 and 2.23.

The detachment coefficient *k_det* is first calculated and then used to define the detachment frequency *nu_det* by multiplying gas density. The detachment rate *Rdet* is then calculated from equation 2.7 and is only valid when negative charge concentration is positive. The ion-ion and ion-electron recombination rates *Rrec_ii* and *Rrec_ei* are calculated through equation 2.14 and 2.13 with the ion-ion recombination coefficient. It is to be noted that the recombination rates are only valid when charge carriers concentration is positive. The ionization and attachment rates *Rion* and *Ratt* are computed through equation 2.5 and 2.9.

The standard lightning impulse voltage is applied in the study with 1.2 µs front time and 50 µs time to half-value on wave tail. Since distortions are superimposed during the rise of the impulse, the front time is interpreted using a substitute line through 30% and 90% point. The time T between 30% and 90% points is used to

define the front time T_f as

$$T_f = 1.67T \tag{3.5}$$

A double exponential function is used to implement the lightning impulse voltage

$$v(t) = V_0 \cdot \eta \cdot \frac{\tau_2}{\tau_2 - \tau_1}(e^{-\frac{t}{\tau_2}} - e^{-\frac{t}{\tau_1}}) \tag{3.6}$$

where V_0 is the desired voltage level, η is a voltage efficiency to increase the function peak value to desired level and τ_1 and τ_2 are characteristics time constants determining rise time and half value time respectively. From [3], the time constants τ_1 and τ_2 are chosen as 405 ns and 68.5 ns for a standardized lightning impulse voltage "1.2/ 50". The waveform with an unit peak value is shown in Fig.3.7.

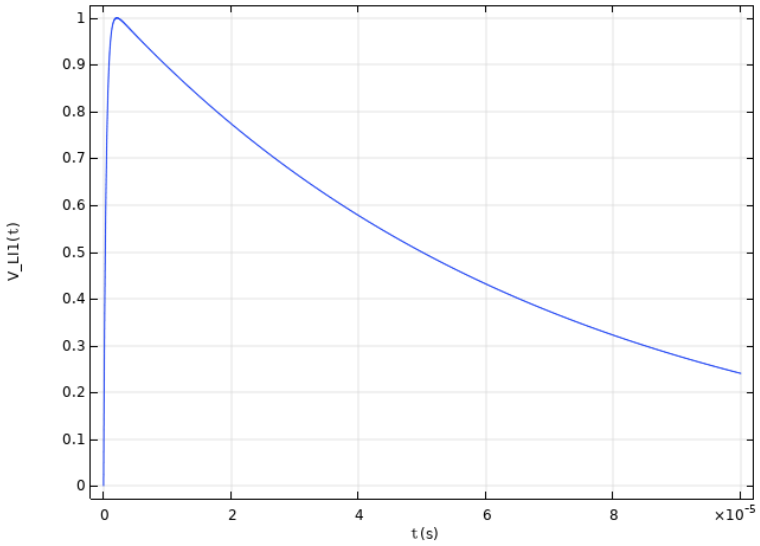

Figure 3.7: *Standard lightning impulse with front time* 1.2 µs *and* 50 µs *time to half-value. The peak value is set as 1 and the duration is* 100 µs

By using the double exponential function, a consecutive lightning impulse series will be constructed using the *Picewise* function as shown in Fig.3.8. The three impulses durations are 150 µs, 200 µs and 250 µs individually. The reason for choosing distinct durations will be discussed in later chapter. Linear functions of 34 µs duration and ends as zero value will be added at the end of each impulses tails which will be followed by a 1 µs manual 'relaxation time'.

All the functions built will then be used to determine the input voltage by multiplying with the voltage magnitude V_{amp}.

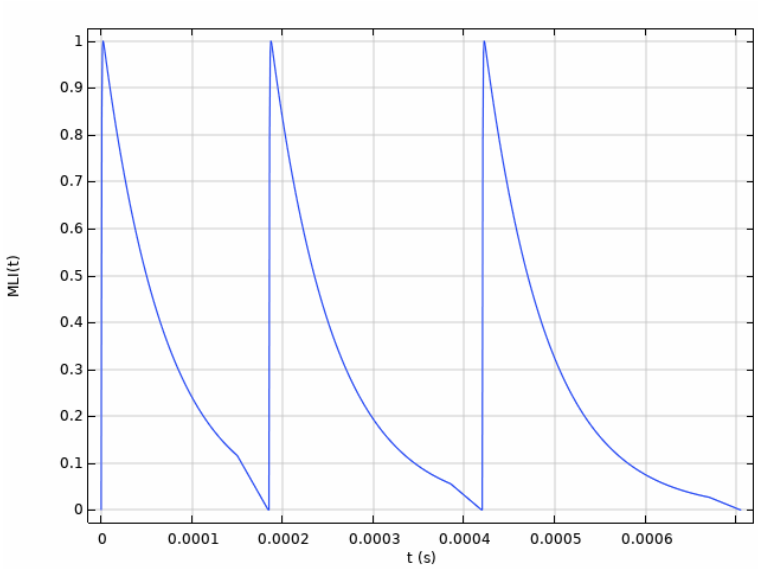

Figure 3.8: *Consecutive lightning impulses with different durations respectively.*

3.4 Finite element mesh

The mesh node discretizes the geometry into small unit of simple shapes and this is one of the challenge in this study since sharp triple junction exists in the geometry even the fillet function has been applied. Besides, the balance between mesh element sizes or computational time and the accuracy of results needs to be kept. With coarse and simpler meshing sequence, the demand of the computational power and time can be reduced but the accuracy of the result will be affected. On the contrary, if extremely fine mesh size is applied to the whole geometry the resulted mesh elements number will be enormous and is impossible to proceed simulation.

The mesh setting is settled after multiple tries on different settings. The air domain near the air gap where discharges emerge and develop is more of interest and thus is assigned with smaller sizes meshes. Based on experience and available information, the element size should be kept small enough (around 20 µm) and uniform at the triple junction region to resolve the high concentration gradient problem. The stress cone, gel, insulator and the rest of air region are assigned with coarser meshes to reduce the number of mesh elements since good resolution is not needed.

As stated in section 3.1, a *Mesh Control Edges* node is used to divide the region near the air wedge. The *size* sub-node calibrated for general physics with custom parameters is assigned to the this air region. The maximum and minimum element sizes are set as 4×10^{-4} m and 1.01×10^{-6} m with maximum element growth rate as 1.018 to define the mesh growing from small elements region to big elements region. The rest of air domain is assigned with extremely fine mesh size using the default *size* sub-node. Besides, another *size* sub-node is defined for the stress cone, gel and insulator domain to reduce the element numbers. The maximum and minimum element sizes are set as 12.4×10^{-4} m and 7.56×10^{-6} m with maximum element

growth rate as 1.3. It is noticed that the air region near the air wedge has the finest element size compared with other region to ensure the accuracy while keep the total elements number at a acceptable level.

Several *Distribution* sub-nodes are added to specify the element sizes along the boundaries which combined with the *size* sub-nodes determine the meshes of the whole geometry. The mesh distribution along curved gel boundary is set as predefined as 100 elements with 1.5 element ratio and arithmetic sequence growth formula in reverse direction. The element ratio determines the growth rate and in our case the area near triple junction is of most interest thus have the smallest element sizes. As for the rounded gel corner, 16 elements are distributed along boundary with 1 element ratio and arithmetic sequence growth formula. The meshes along vertical stress cone boundary have 500 elements allocated with 3 element ratio and grow in arithmetic sequence. It is noted that since the vertical boundary is much longer than the gel boundary and thus more element numbers are assigned and bigger element ratio is used to reduce the element numbers at the top of vertical stress cone boundary. The resulted mesh owns 50596 domain elements and 1133 boundary elements. The resulted mesh is shown in Fig.3.9.

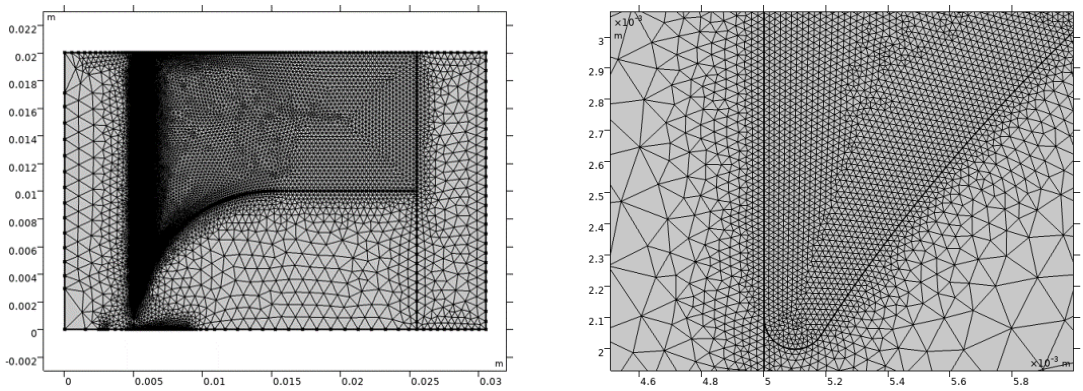

(a) *Mesh for the overall geometry.* **(b)** *Mesh for the critical region.*

Figure 3.9: *Mesh setting for the overall computational domain and the critical region. Smaller size elements are assigned to the critical region where charging behaviours are expected.*

The setting discussed above is for the scaled-down 2D geometry. For the 2D model with one air wedge, the element size setting is the same as the scaled-down case and different boundaries distributions are applied. The *Distribution* setting for boundaries are set as fixed number of elements with 350 for curved gel boundary, 15 for rounded gel corner and 500 for the vertical boundary. This gives 29546 domain elements and 1083 boundary elements.

3.5 Calculations of the discharge current

The calculation of the discharge current in 1D model has been thoroughly discussed in [2], the main focus will be on the calculation in 2D model. A local variable is

defined under *Component* as J_{cap} which is the displacement current density. Since no major ionic conduction in the insulating material, the displacement current component will be a good indication of the discharge. The integral *Boundary Probe* sub-node is added and assigned to the voltage applied stress cone boundary. It is used to calculate the displacement current collected at the boundary and the expression input is J_{cap} while the integral setting is kept as default. In this way, the displacement can be monitored.

4

Results and Discussion

In this chapter, the modeling results are provided and discussed. First of all, a coaxial 1D model expanded from previous works [2] is studied to investigate the charging behaviour under standard lightning impulse voltage in a two air gaps and three solids geometry representing the critical region of the air-polymeric interface. The influence of stabilization method on the simulation accuracy is also reviewed. Thereafter, the developments of corona discharges are inspected in 2D models in which discriminated gel heights are implemented and different voltage levels and polarities are imposed. An observation of the charging behaviours under consecutive lightning impulses is conducted later with the anticipation of collected surface charge affecting the charging behaviours. The decay of accumulated surface charge is then inspected to supplement the discussion.

It is to be noted that mostly the qualitative investigations are conducted in this study since the model is simplified from the real product. The phenomenons and behaviours are the main focus compared with numerical values which holds a huge uncertainty due to the uncertainties of model parameters as well as the limited amount of experimental inputs for validation.

4.1 1D Model

To be able to ensure the functionality of the model under standard lightning impulse voltage and to inspect the influence of stabilization method used, a coaxial 1D model with three solids two gases domains is set up. Simulation with 1D model should be less time consuming and will act as a good starting point for understanding the basic concepts of the discharge dynamics.

In chapter 3, the simplification from target object towards 1D model in a coaxial system is introduced. As shown in Fig.4.1, the five domains from left to right represent stress cone, air, gel, air and insulator. For the convenience of characterization, the left and the right air domains are labeled as 'Domain 1' and 'Domain 2' respectively. The four interfaces between air and surrounding insulators are also marked separately.

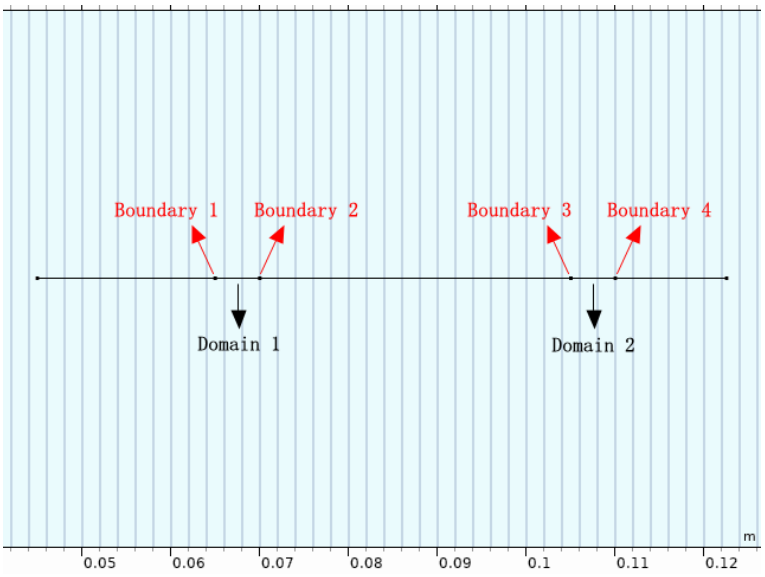

Figure 4.1: *Labeling of 1D simulation model geometry. Two air domains and four interfaces between air and insulators are marked.*

4.1.1 Corona Discharge

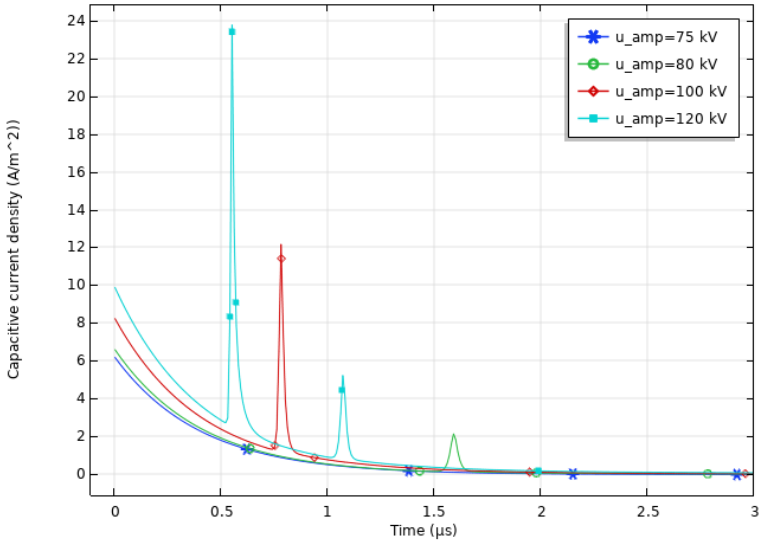

Figure 4.2: *Capacitive current densities at the ground side for* $+75\,\mathrm{kV}, +80\,\mathrm{kV}, +100\,\mathrm{kV}$ *and* $+120\,\mathrm{kV}$*. Discharge initiate at around* $+80\,\mathrm{kV}$*.*

A sweep analysis on applied voltage magnitudes is conducted with the voltage levels of $+75\,\mathrm{kV}, +80\,\mathrm{kV}, +100\,\mathrm{kV}, +120\,\mathrm{kV}$. The voltages are chosen from a tryout process. The capacitive current density J_{cap} collected at the ground side for each case is shown in Fig.4.2. At the voltage level of $+80\,\mathrm{kV}$, a small peak emerges at around $1.59\,\mu\mathrm{s}$ which indicates a rapid change of electric field due to the initiation of ionization or a small discharge on the interface. Since no such phenomenon is observed for $+75\,\mathrm{kV}$, $+80\,\mathrm{kV}$ can be treated as the onset voltage for the discharges. Much higher

peaks are noted at the voltage levels of +100 kV and +120 kV indicating stronger discharges under these voltage levels. This is predictable since higher voltage levels result in higher electric field strength that will lead to more intensive ionization collisions.

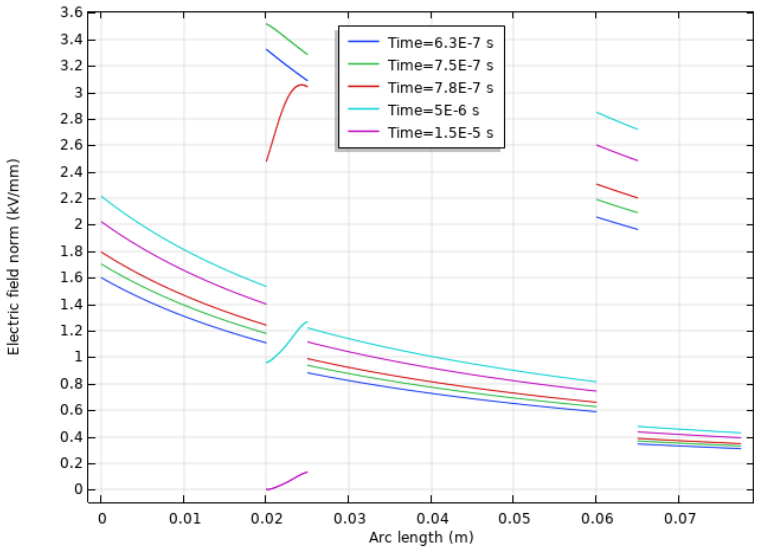

(a) *Electric field strength.*

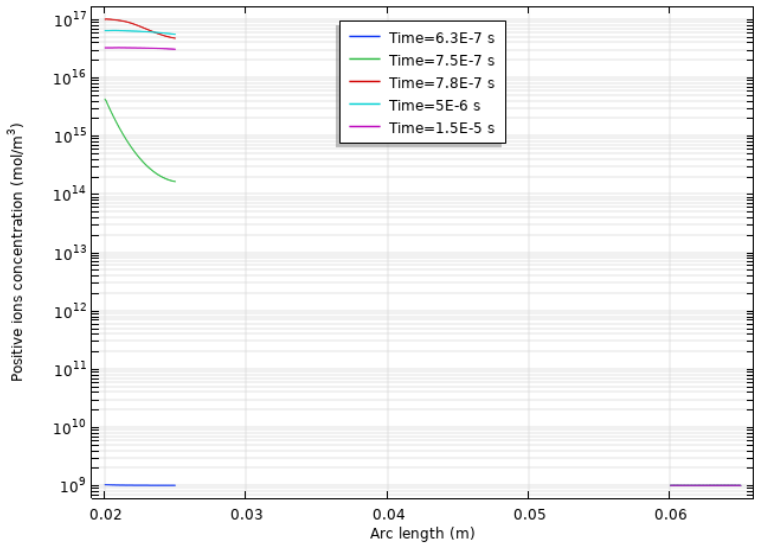

(b) *Positive ions concentration.*

Figure 4.3: *Electric field strength and positive ions concentration in log scale under the lightning impulse voltage of* +100 kV*. Localized discharge in domain 1 can be observed.*

The discharge appears at around 0.78 µs at +100 kV LI. The electric field strengths in the entire geometry before and after the discharge are shown in Fig.4.3a. The five plot groups from left to right represents the electric field in stress cone, air domain 1, gel, air domain 2 and insulator. The electric field strength in stress cone, gel and insulator is gradually increasing with the voltage rising, but still lower than the

field in the gas media because of the field displacement phenomenon. In domain 1, the electric field increases until 0.75 µs and is higher than 3 kV mm^{-1} which is the typical breakdown strength of air. A complete breakdown will not take place since the electric field strength in solids are not high enough to cause a punctuation. The discharge is localised in domain 1 and after the discharge the electric field decreases intensely due to the field distortion by the remaining charge carriers in the air. Moreover, the electric field in domain 2 is not high enough to initiate a discharge due to the coaxial geometry.

In Fig.4.3b, the group of lines at the left side indicates the positive space charge change during the discharging process in domain 1. In accordance with discussion above, the positive space charge concentration increases from a initial concentration of 10^9 mol m^{-3} to 10^{17} mol m^{-3} within a very short time which indicates an intensive ionization in the gas. At a later time instant, the concentration of positive ions shows a slight decrease which is related to recombination process and accumulation at the gel surface. If we only consider the drift motion in the air gap with the assumption of a constant electric field strength of 3 kV mm^{-1}, the time needed for a positive ions travel through the whole region is around 8.33 µs from equation2.2. However, since the field decrease rapidly after the discharge, the actual time for all the space charges to be swept out will be much longer. It is conspicuous that the positive space charge concentration in domain 2 barely changes suggesting that the ionization only appears in domain 1 under this voltage level.

For a higher voltage level of +120 kV, two peaks can be observed at around 0.55 µs and 1.07 µs respectively. As shown in Fig.4.4a, the electric field strength for initiating discharges is higher than 100 kV case. Similar growth of positive ions can be observed in domain 1 which represents the first peak of capacitive current density. It's worth noting that after the first discharge, the electric field strength in domain 2 increases to around 3.2 kV mm^{-1} which is higher than previous case and thus results in a second discharge in domain 2. Such secondary discharge can be noticed in Fig.4.4b with concentration of positive space charge increase intensely after 1.03 µs. In conclusion, with higher voltage level more intensive discharge can be observed in domain 1 and additional discharges will emerge in domain 2 given the voltage level is high enough.

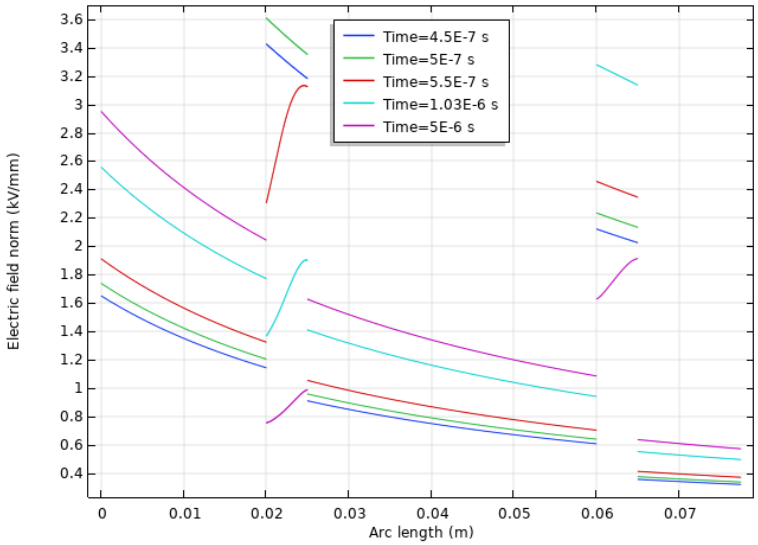

(a) *Electric field strength.*

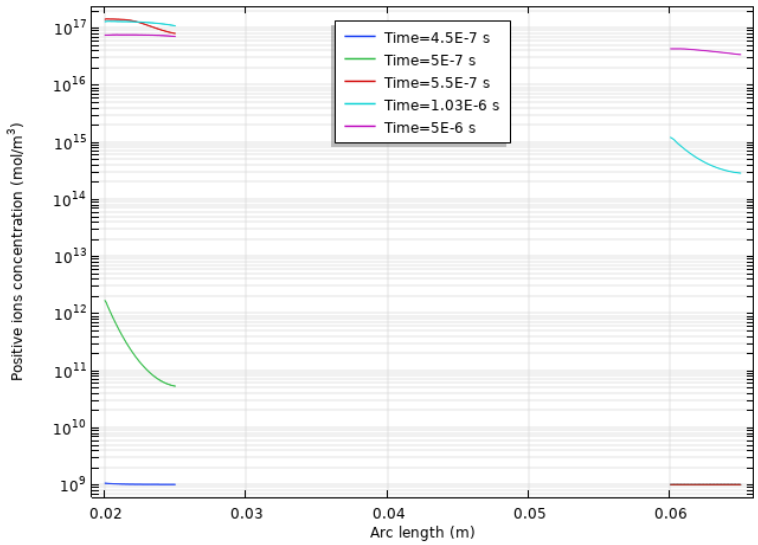

(b) *Positive ions concentration.*

Figure 4.4: *Electric field strength and positive ions concentration in log scale under the voltage of* +120 kV*. Discharges emerge in both domain 1 and domain 2.*

Surface charge accumulation is another major topic related to charging behaviour. After the occurrence of discharge, the high concentration of charge carriers will be drifted towards the boundaries and then accumulated on them. The positive charge carriers will be drifted in the direction of electric field and accumulate on boundary 2 and 4 while negative charge carriers will move in the opposite direction and are collected on boundary 1 and 3. As shown in Fig.4.5a, under +100 kV two main increase of surface charge are observed on boundary 2. The first growth till around 0.73 µs is rather tardy since not too many charge carriers are in the air domain and the drifting process is restricted. A rapid increase appears afterwards because of the discharge process that the generated positive space charges will accumulate on

the boundary. After the discharge, the remaining charge carriers will be gradually drifted towards the boundaries. Since no discharge emerges in domain 2, no sharp growth of surface charge can be obtained. However as discussed before, secondary discharge exits in domain 2 under the voltage level of +120 kV which will lead to a sharp increase of surface charges on boundary 2. Besides, more intensive discharge will generate higher amount of charge carriers that will converted to surface charge. Therefore, more surface charge is collected on boundary 1 for 120 kV LI.

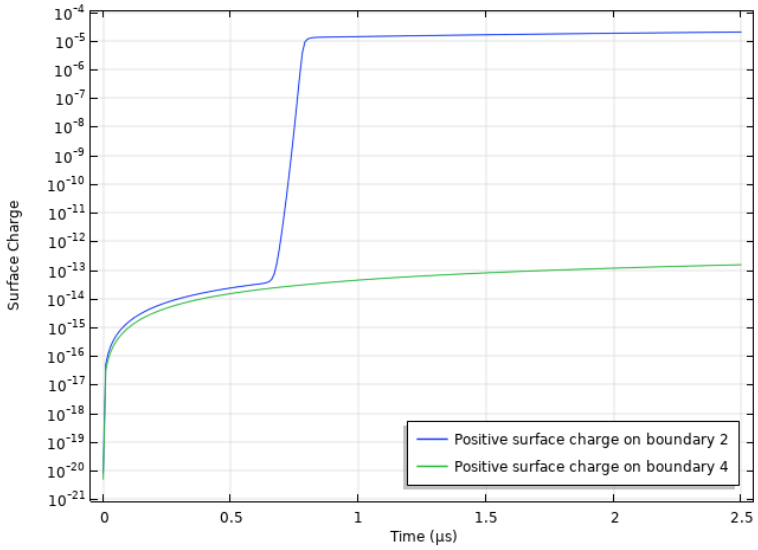

(a) *Surface charge accumulation for* +100 kV*.*

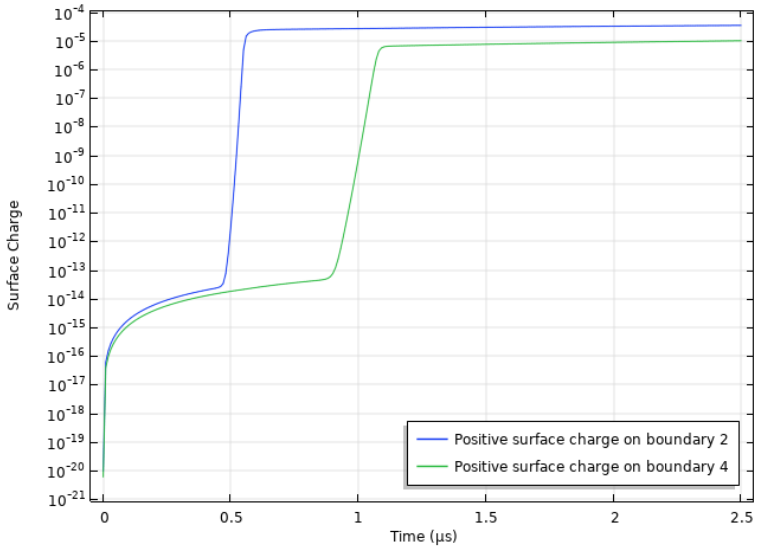

(b) *Surface charge accumulation for* +120 kV*.*

Figure 4.5: *Positive surface charge accumulation in log scale on boundary 2 and boundary 4 under the voltage of* +100 kV *and* +120 kV*. Positive ions produced by discharges will be accumulated on boundary 2 and 4.*

Similar increase of negative surface charges on boundary 1 and 3 will be observed. Positive surface charge on boundary 2 and negative surface charge on boundary 1 in

domain 1 under the same voltage of +100 kV is shown in Fig.4.6. Negative surface charges have earlier increase after the discharge which is related to the high mobility of electrons compared with other charge carriers. Electrons will be drifted to and collected on boundary 1 before the ions can arrive at related boundaries.

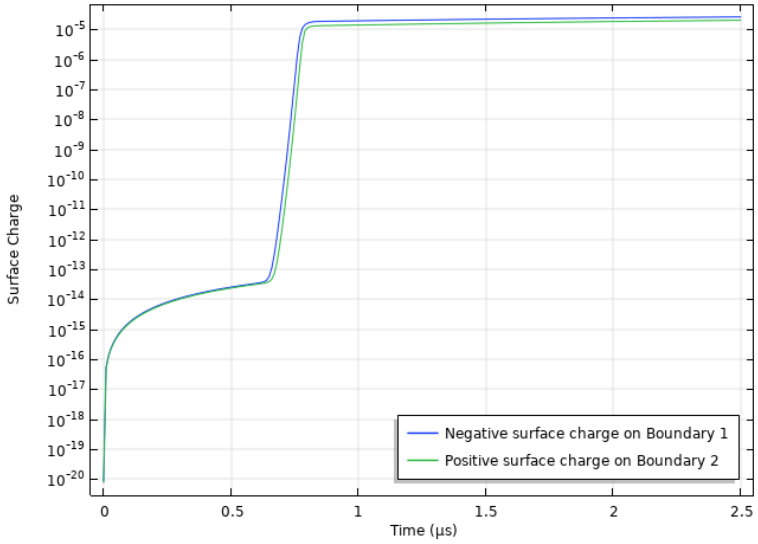

Figure 4.6: *Negative surface charge on boundary 1 and positive surface charge on boundary 2 in log scale under the voltage of* +100 kV*. Negative surface charges start increasing earlier due to the high electrical mobility of electrons.*

4.1.2 Stabilization method

Large concentration gradient will cause convergence problem in the solutions.As discussed in chapter 3, special stabilization technique is implemented to resolve the unstable discretized problems. However a balance between stabilization and accuracy should be reached that the tuning parameter can not be too high otherwise the artificial diffusion will tamper the solution.

A sweep analysis over the artificial diffusion parameter ad_p is conducted under +160 kV with the values of 0.1, 0.5 and 0.9 under. The reason for choosing such high voltage level is to intensify the discharges and increase the concentration gradient of charge carriers in the air domain. The electron concentrations in air domain 1 and 2 are shown in Fig.4.7a and 4.7b with $ad_p = 0.1$ and $ad_p = 0.5$. For a small tuning parameter of 0.1, unphysical negative concentration is observed in domain 2 which appears as discontinues line in log scale in Fig.4.7a. Such problem can be resolved with using a higher artificial diffusion parameter to sweep out the electrons and smooth up the concentration as shown in Fig.4.7b.

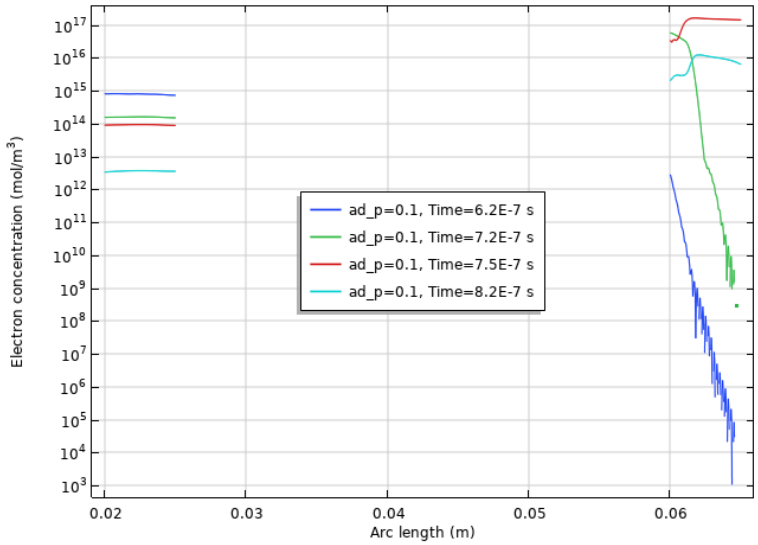

(a) *Electrons for* $ad_p = 0.1$.

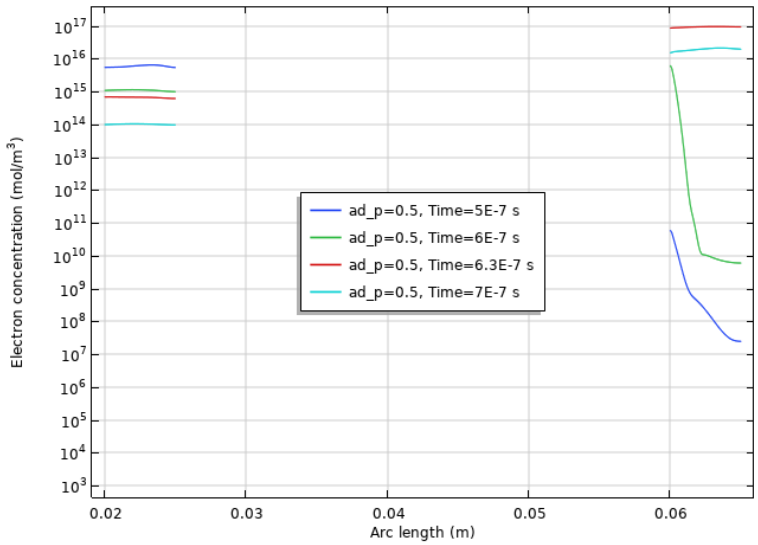

(b) *Electrons for* $ad_p = 0.5$.

Figure 4.7: *Electron concentration in log scale in domain 2 for* $ad_p = 0.1$ *and* $ad_p = 0.5$ *under* $+160\,\mathrm{kV}$. *The high concentration gradient will lead to un-physical results which can be improved with artificial diffusion added.*

In Fig.4.8 the capacitive current densities for three cases are illustrated. It is noted that the first peak of capacitive current density indicating discharge in domain 1 deviates slightly but small oscillation in second discharge is smoothed out with higher tuning parameter. Nevertheless, solution is distorted for bigger tuning parameters. If the artificial diffusion is too high, the results will be deviated greatly as the second discharge for the $ad_p = 0.9$ case. This is because the artificial diffusion implemented affects the physical diffusion processes too much.

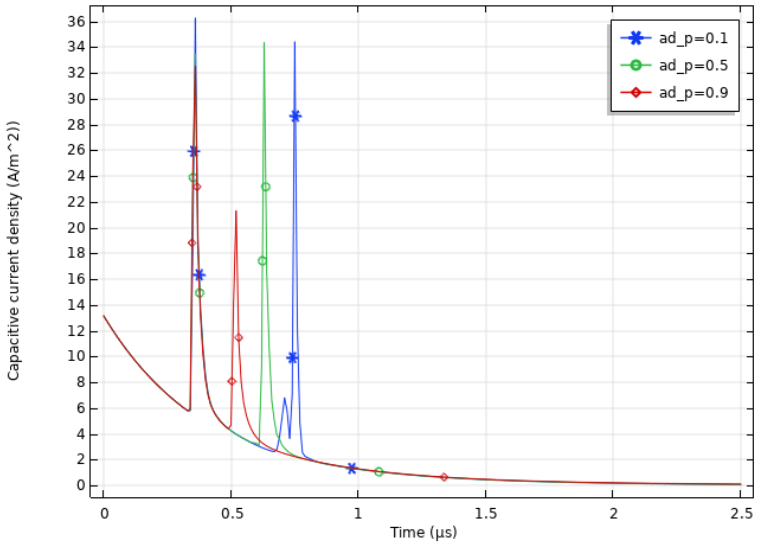

Figure 4.8: *Capacitive current densities at the ground side for tuning parameters of* $0.1, 0.5$ *and* 0.9 *under* $+160\,\mathrm{kV}$. *Results will be distorted given tuning parameters too high.*

4.2 2D model

From the results of 1D model, the basic understandings of charging behaviours have been obtained. The focus now turns to 2D model. One air wedge rather than two air wedges 2D models are used in our simulation in order to avoid the complexities of geometry and mesh settings. On the other hand, the rear side air wedge which endures lower electric field strength because of the coaxial structure in the product holds low possibility of discharge and thus is of less interest.

The connected gel, stress cone and air will form a sharp triple junction which suffers the highest field strength and therefore is the region where discharges are most likely initiated. A 2D geometry with smoothed triple junction and the consideration of wetting effect of the gel is utilized. The corona discharges and charge accumulation will be investigated and the influences of voltage levels and polarities are to be determined in Section 4.2.1. Thereafter, the decay of accumulated surface charges and surface charge impacts on discharging behaviour are studied using a scaled-down 2D model in Section 4.2.2 to reduce the exaggerated computational power and time required. Short conclusion will be made at the end of each subsection to illustrate the main findings.

4.2.1 2D model with a rounded triple junction

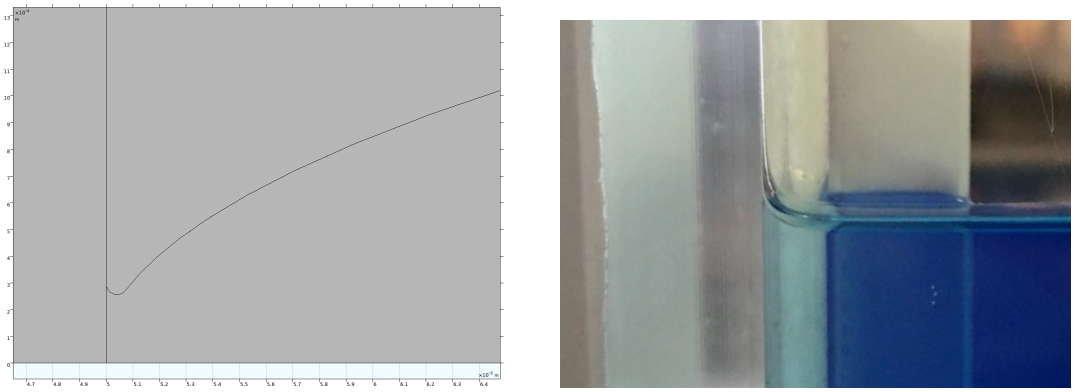

(a) *Rounded triple junction geometry.* **(b)** *Triple junction in experiment test cell.*

Figure 4.9: *Rounded triple junction geometry used and triple junction in test set up. The rounded corner conforms more with the set up.*

As illustrated in Fig.3.2a and Fig.4.9, the used triple junction is rounded. The geometry conforms to the experimental observation that the gel climbs up the insulator surface. It also avoids sharp edges in the geometry that will cause convergence problem and meshing difficulties. The gel height is kept as 3 mm from the bottom boundary. A lightning impulse of +120 kV is first applied to demonstrate how the corona discharge initiate and develop. Comparisons with cases at lower voltage level, with higher gel height and negative polarity lightning impulse are conducted separately and presented in later sections.

4.2.1.1 Corona discharge in 2D model

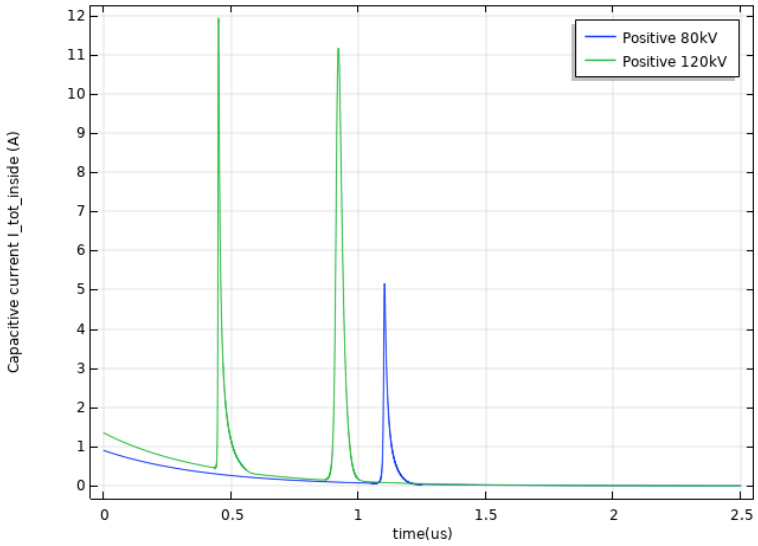

Figure 4.10: *Capacitive current for* +80 kV *and* +120 kV *lightning impulse voltage with the gel height of* 3 mm. *Higher voltage level will cause more intensive discharges.*

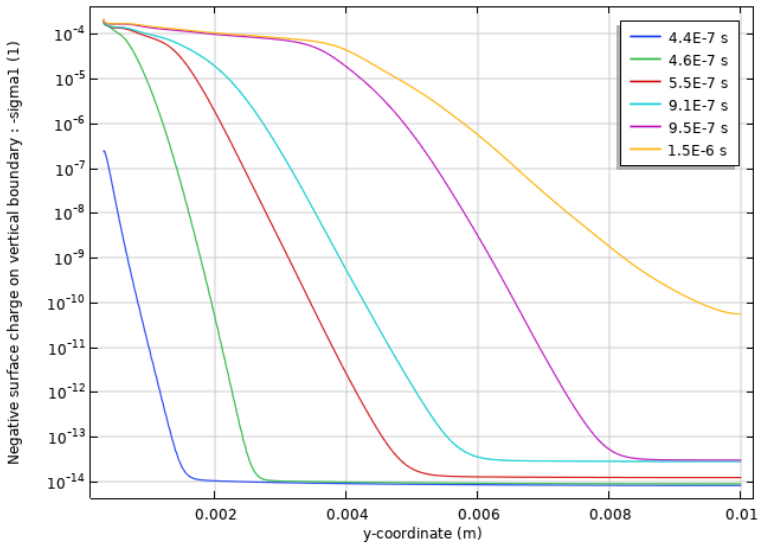

Figure 4.11: *Negative surface charges on vertical boundary in log scale under lightning impulse voltage of* +120 kV *with the gel height of* 3 mm. *Accumulation occurs after the discharges.*

From Fig.4.10, two peaks can be observed at around 0.46 µs and 0.92 µs respectively under the voltage of +120 kV. The charge carriers and electrons will be drifted by the background field and accumulate at the interfaces, in the same way as already being observed in the 1D model. Positive surface charge will be accumulated at the curved boundary while negative charges will accumulate at the vertical boundary

shortly after the discharge. Since no surface charge transport model is considered in this study, the surface charge will not move along the interface and will remain in the same place on the boundary. In Fig.4.11, the negative surface charges at the vertical stress cone boundary are illustrated in log scale. After the first discharge, the surface charge gradually accumulates especially at the lower region where discharge happens. Noticeable increase at higher part of boundary can be observed after the second discharge.

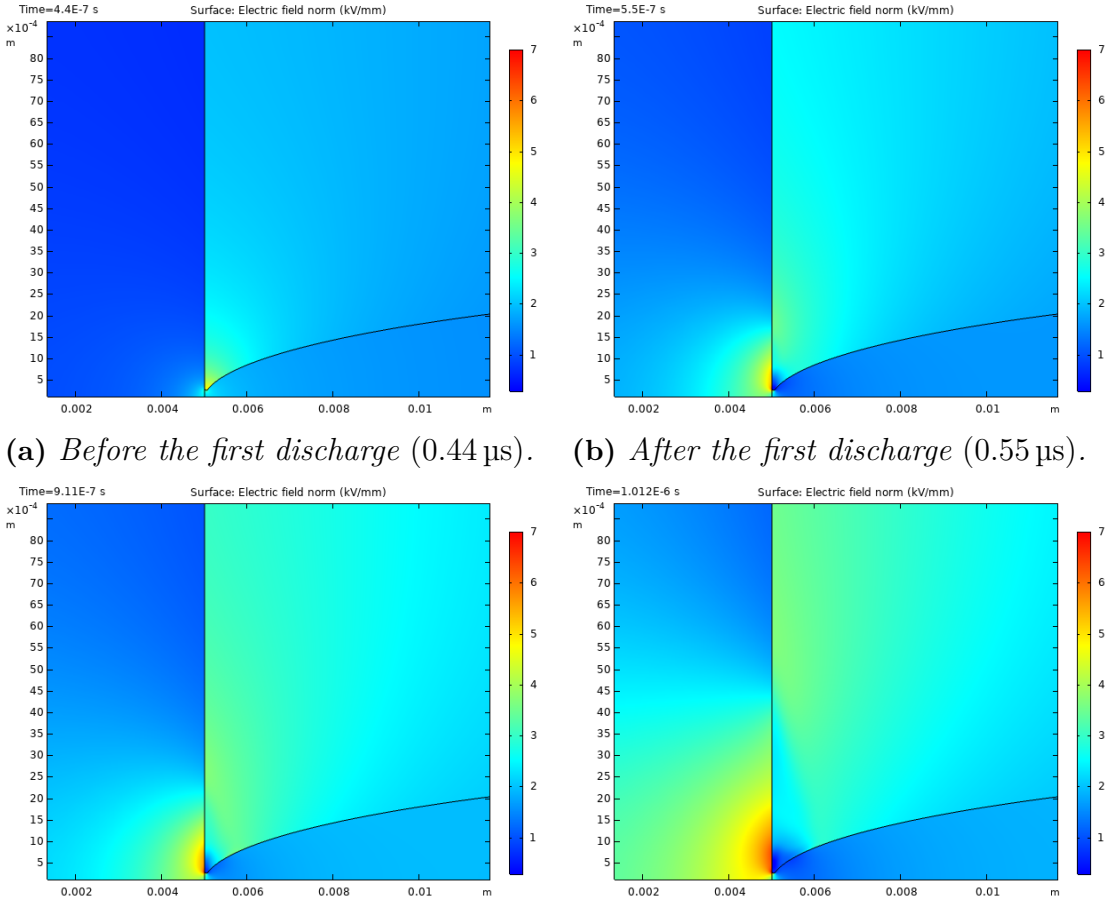

(a) *Before the first discharge* (0.44 µs). **(b)** *After the first discharge* (0.55 µs).

(c) *Before the second discharge* (0.91 µs). **(d)** *After the second discharge* (1.01 µs).

Figure 4.12: *Electric field strength for four time instants under* +120 kV *with* 3 mm *gel height. Discharge emerges in region around triple junction and high field region obtained along vertical boundary.*

The nominal electric field strength and positive ions concentration surface plots for four time instants before and after the discharge are shown in Fig.4.12 and Fig.4.13. The electric field strength at the region around triple junction rises to about 4.5 kV mm^{-1} at 0.44 µs that initiation of ionization can be observed in Fig.4.13a and the first discharge emerges later at around 0.46 µs. After the discharge, the electric field strength is reduced in lower region because the existing space charges generate a field in the opposite direction of the background field within the discharged area. Thus, a higher electric field strength will be obtained above the discharged low field region and will gradually increases with the rising applied

voltage. At around 0.91 µs, the electric field in upper area is around 4.5 kV mm^{-1} that a second discharge occurs at the region above the first discharge part. The high field region switched to even higher area but the field strength is not high enough for more discharges.

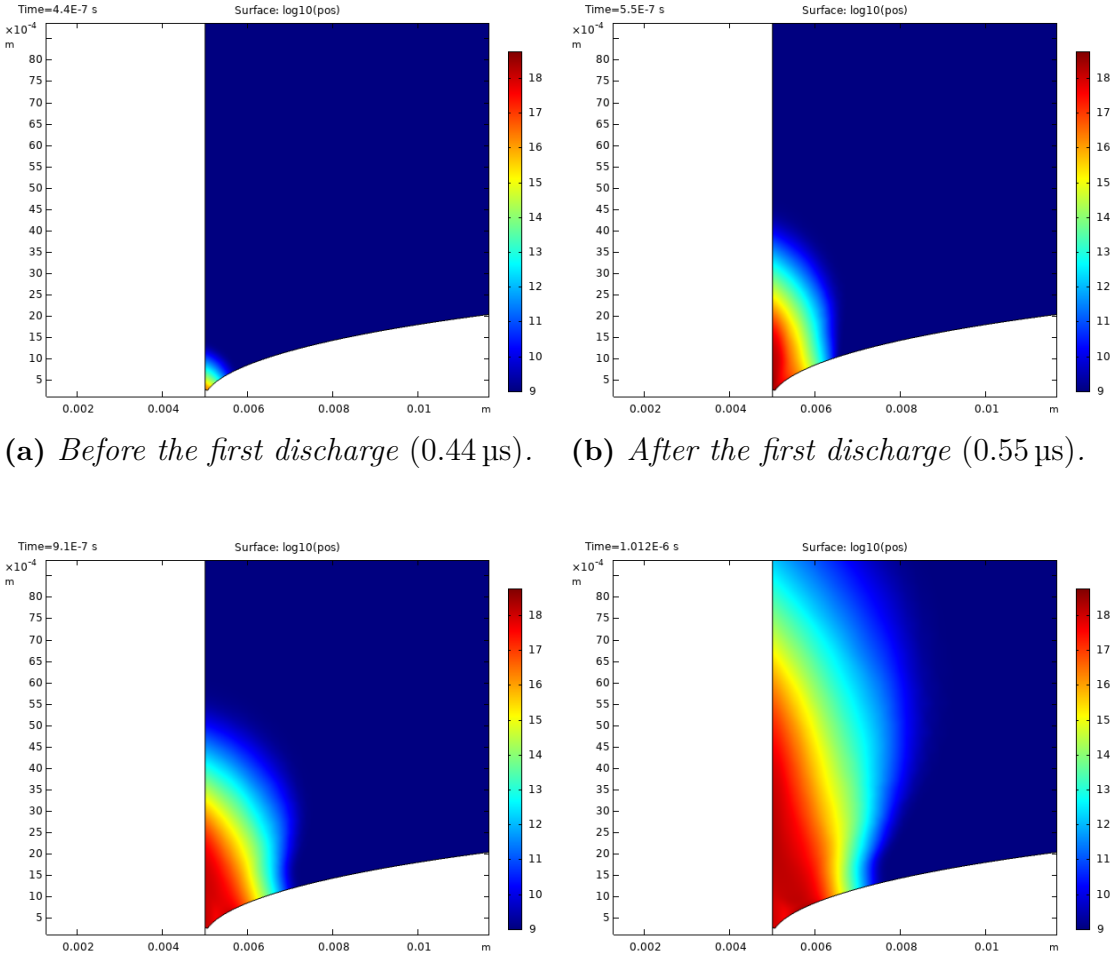

(a) *Before the first discharge* (0.44 µs). **(b)** *After the first discharge* (0.55 µs).

(c) *Before the second discharge* (0.91 µs). **(d)** *After the second discharge* (1.01 µs).

Figure 4.13: *Positive ions concentration in log scale for four time instants under* +120 kV *with* 3 mm *gel height. Positive ions are generated by discharges and drifted in the direction of the electric field.*

In Fig.4.13, the alteration of positive space charges concentrations is shown clearly. After the first discharge, high amount of positive space charges appear in the lower region. When the second discharge occurs, more positive space charges are generated at upper parts and gradually drifted outwards by the background field. It is noted that the discharge shows a behaviour of 'propagating' along the vertical boundary between the stress cone and air where holds high electric field strength.

4.2.1.2 Influence of voltage level and gel height

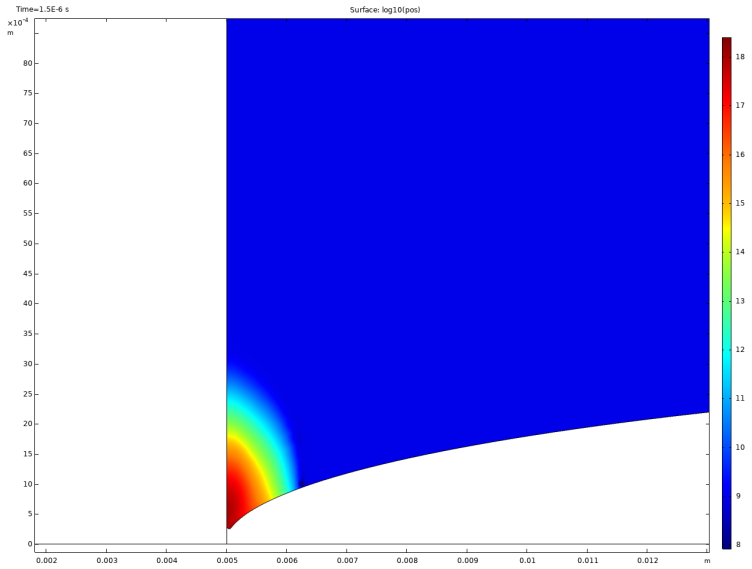

Figure 4.14: *Positive ions concentration after discharge under impulse voltage of* +80 kV *with* 3 mm *gel height. Discharge restricted in lower region.*

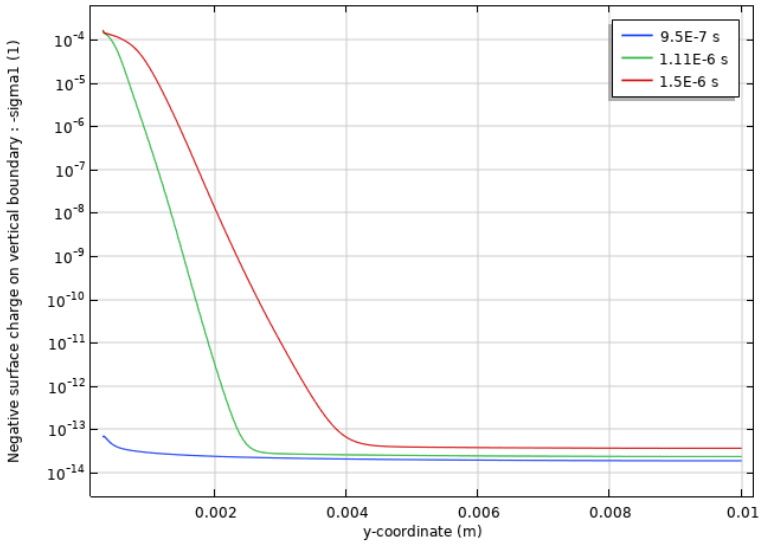

Figure 4.15: *Negative surface charge on vertical boundary in log scale under* +80 kV *with* 3 mm *gel height. Lower concentration negative charge on stress cone surface for* +80 kV.

Discharges under different voltage levels and gel heights are to be investigated in this section. For a lower voltage level of 80 kV, one smaller discharge can be observed around 1.102 µs from Fig.4.10. The positive space charge concentration after discharge is shown in Fig.4.14. The discharge region is restricted at the lower part of the wedge and no further discharge occurs at upper part compared with +120 kV

case. This is predictable since the electric field above the discharged is not strong enough under this voltage level. Similarly, the negative ions will be drifted to the vertical interface between stress cone and air and then accumulated as shown in Fig.4.15. The negative charges gradually accumulated at the vertical boundary after the discharge. However, the concentration is noticeably lower for higher boundary compared with Fig.4.11. Thus with higher voltage applied, more charges can be generated and accumulated on the boundaries.

At even higher voltage level, the discharge can be strong enough to enhance the field due to the developed space charge. This might result in a propagating dis- charge into the air region. The space-charge-dominated streamer discharge forms conducting paths of long distance with rapidly increasing ionizing collisions. This will lead to extremely high concentration and concentration gradient of charge species that will cause convergence problem to current simulation set up. No streamer physics is included in our model in order to reduce the complexity of the model. For extreme high voltage level, the emerged convergence problems will be treated as indication of streamer discharges in the system by combining with close inspection of the space charge distribution.

In the present studied 2D geometry such numerical behaviors have occurred at voltages of 130 kV and above. That is a strong indication that a flashover in the air volume above the gel surface (or along the gel surface) between the stress cone and the inside of the outer insulator emerges at this level. In this case the discharge critical voltage is 130 kV which is higher than the discharge onset voltage at around 80 kV.

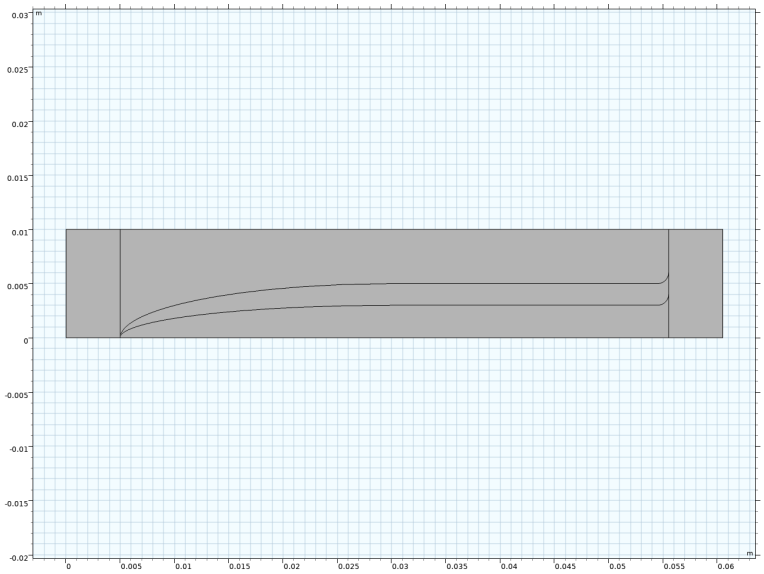

Figure 4.16: *Rounded edge 2D model geometries with gel height of* 3 mm *and* 5 mm. *Higher gel surface will stress the air around triple junction more.*

The charging behaviour in a higher gel model is also investigated and compared under the same voltage level of +80 kV. As shown in Fig.4.16, a model with the gel

height of 5 mm is introduced. The capacitive current and negative surface charge accumulated at vertical boundary is illustrated in Fig.4.17. The air wedge will be narrower for higher gel, thus the triple junction will be stressed with higher electric field strength as discussed. A small second discharge can be observed at 0.75 µs for 5 mm case. Compared with Fig.4.15, higher surface charge accumulation can be observed at higher region because of the secondary discharge.

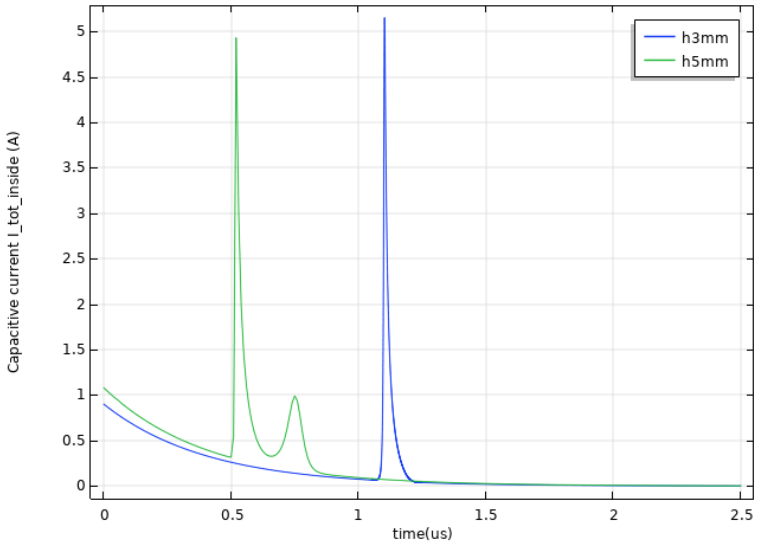

(a) *Capacitive current.*

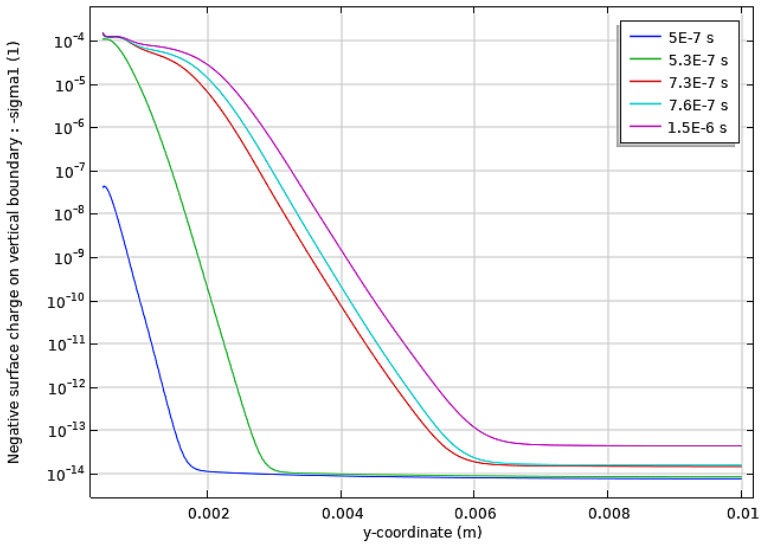

(b) *Negative surface charge for* 5 mm.

Figure 4.17: *Capacitive current and negative surface charge in log scale for* 3 mm *and* 5 mm *gel heights under*+80 kV *LI. Higher gel surface will intensify the discharges.*

4.2.1.3 Influence of voltage polarity

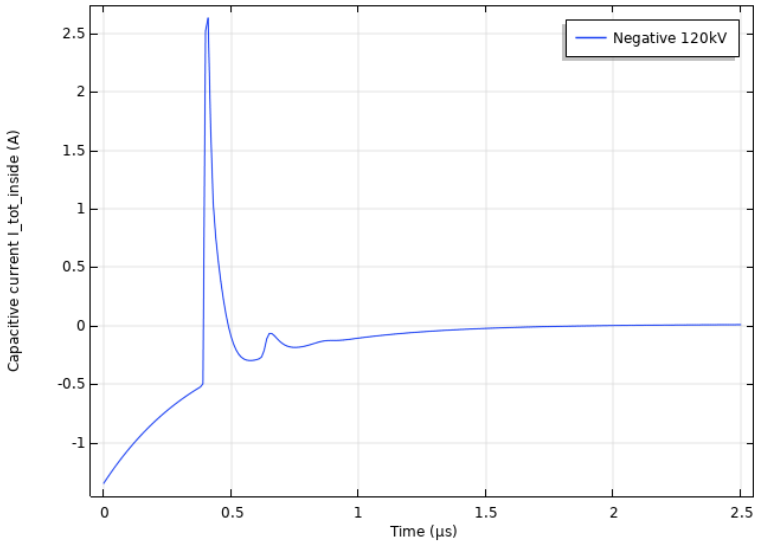

Figure 4.18: *Capacitive current for voltage of* $-120\,\mathrm{kV}$ *with* $3\,\mathrm{mm}$ *gel height. Discharge occurs at around* $0.41\,\mu\mathrm{s}$.

The impact of voltage polarity is studied with the voltage of $-120\,\mathrm{kV}$ to compare with the previous case of $+120\,\mathrm{kV}$ on the $3\,\mathrm{mm}$ gel height model. As shown in Fig.4.18, a peak at around $0.41\,\mu\mathrm{s}$ indicating a discharge in the air is observed. The displacement current starts at negative values which is due to the current being collected at low potential side under negative polarity.

The electric field strength surface plots before and after the discharge are shown in Fig.4.19. A field strength around $4.5\,\mathrm{kV\,mm^{-1}}$ is obtained at $0.39\,\mu\mathrm{s}$. Such high strength will lead to a discharge in the low region around triple junction and the generated space charge will distort the background field. High field strength will lay along the curved gel surface outside the discharged area and also gradually increases with the applied voltage.

It is notable that compared with positive polarity cases, the discharge is developing along the curved gel surface rather than the vertical boundary. This is because of the high electrical mobility of the electrons that its movement determines the direction of ionization. The electrons are drifted in the opposite direction with the field and will move from air towards the gel surface under the negative polarity. Moreover, electrons and negative ions from attachment process will accumulate on the gel surface in negative polarity case shortly after the discharge and will stress the gel. If we compare Fig.4.12d and Fig.4.19d, it is obvious that the stress cone is stressed with higher field in positive case while the gel is stressed when negative polarity voltage applied. Thus the direction of discharge also affects the field distribution in insulation materials.

The distribution of positive ions in Fig.4.20 is also in accordance with the discharge direction mentioned. Initiation of discharge can be observed at the lower region around triple junction while the concentration gradually increases along the curved gel surface. The positive ions are later drifted in the same direction of the field towards the vertical interface.

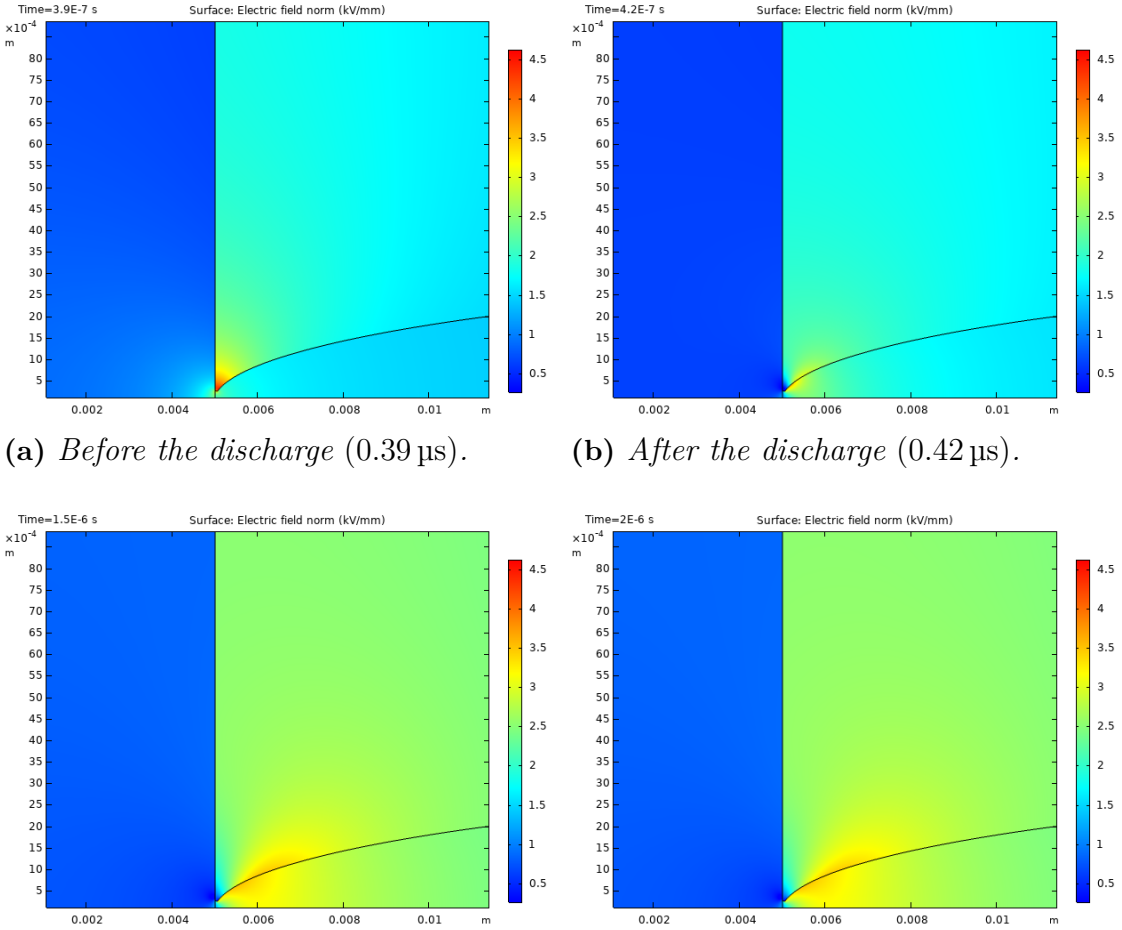

(a) *Before the discharge* (0.39 µs). **(b)** *After the discharge* (0.42 µs).

(c) *Long after the discharge* (1.5 µs). **(d)** *Long after the discharge* (2.0 µs).

Figure 4.19: *Electric field strength in four time instants for* −120 kV *with* 3 mm *gel height. Gel will be stressed with high electric field strength compared with positive case.*

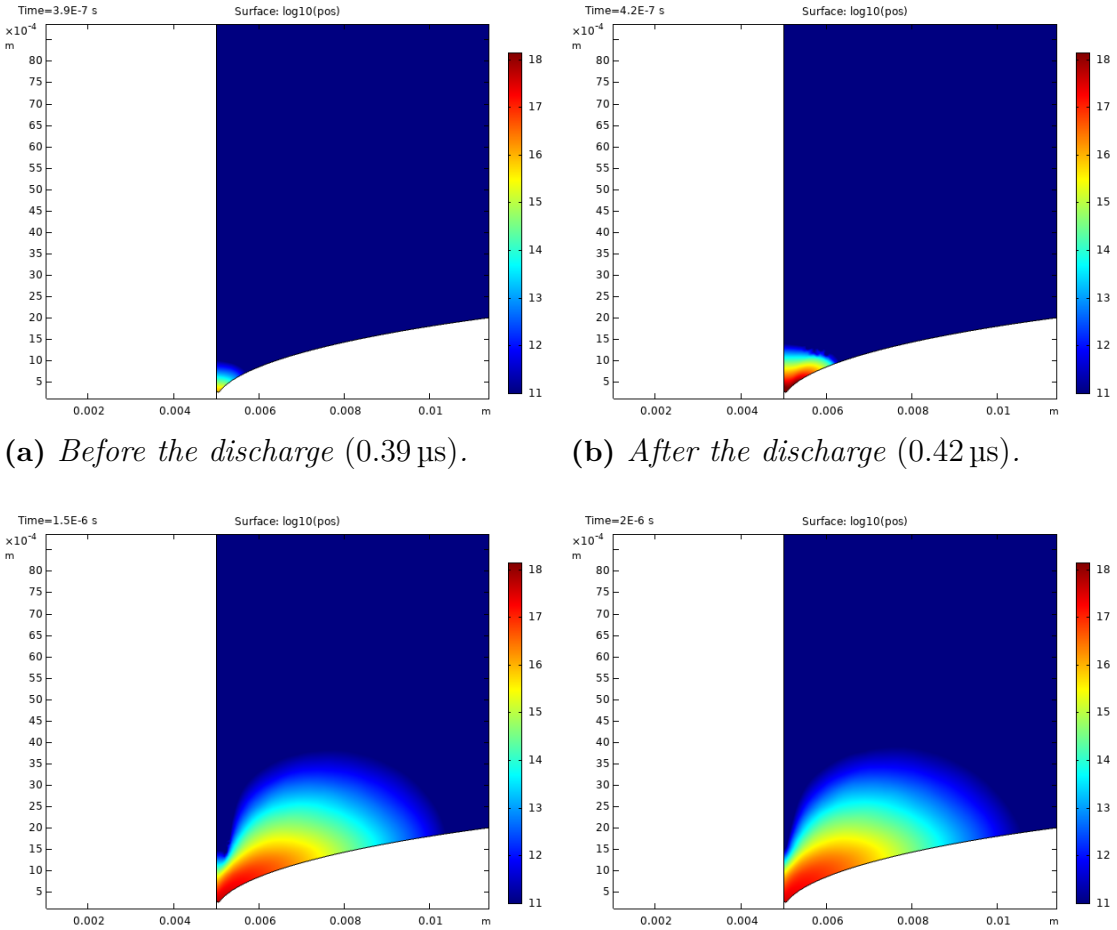

(a) *Before the discharge* (0.39 µs). **(b)** *After the discharge* (0.42 µs).

(c) *Long after the discharge* (1.5 µs). **(d)** *Long after the discharge* (2.0 µs).

Figure 4.20: *Positive ion concentration in log scale at four time instants for* −120 kV *with* 3 mm *gel height. Discharge develops along the gel for negative polarity voltage.*

4.2.1.4 Conclusion

In this section, a number of observations on the charge dynamics are made in the used geometry with distinct impulse voltages applied. Some of the main findings in this section are summarized as follow:

1. Localized discharge deep down in the air wedge can be observed at the discharge onset voltage 80 kV. At higher voltage level, a secondary discharge occurs and develops higher up in the air wedge.

2. The discharges higher up in the air wedge are more dangerous since it may escalate into a propagating streamer discharge along or above the gel top surface which will bridge the stress cone and outer insulator. However, the present model is not suitable for studying this type of fast flashover event that no quantitative statement and further investigation can be made.

3. At the same voltage level, a deeper air wedge will lead to a stronger discharge compared with the shallower wedge. In the studied case, a double discharge occurs with 5 mm wedge while only a single discharge observed with 3 mm wedge.

4. An unsymmetrical behaviour with respect to impulse polarity is observed. This is due to the high electrical mobility of the electrons in contrast to the much lower electrical mobility of the positive and negative space charges.
   - Under positive polarity, the stress cone surface is strongly charged that higher field strength is stressed in the stress cone.
   - Under negative polarity, the gel surface is strongly charged and the curved gel will suffer from high field strength.
   - In both cases the surface charge strongly distort the field distribution and the locations of the discharges in the air wedge.

4.2.2 Scaled-down 2D model

In previous cases, the simulation time range is restrained to 2.5 µs which is extremely short compared with the relaxation time of 30 s to 60 s between impulses in standard lightning impulse test. To investigate the surface charge decay process and charging behaviours under consecutive lightning impulses, longer simulation time is required which results in huge demand in computational power and time. Certain simplifications and assumptions should be made in this sense. The scaled-down geometry with smaller size and a 8 mm air wedge is proposed and shown in Fig.4.21. The smaller size of the geometry implies lower demand on computational power and time consumption and ensures the possibility of using finer mesh settings around the critical region. The deeper air wedge is advantageous for inspecting the accumulated surface charge distribution along interfaces. Such narrow air wedge also means discharges will emerge at lower voltage levels, as already observed in Sec 4.2.1. It is to noted that the scaled-down 2D model have a distance between potential and ground of 30 mm compared to 60 mm in the previously used 2D geometry. This change in length scale will obviously affect the discharge initiation voltage.

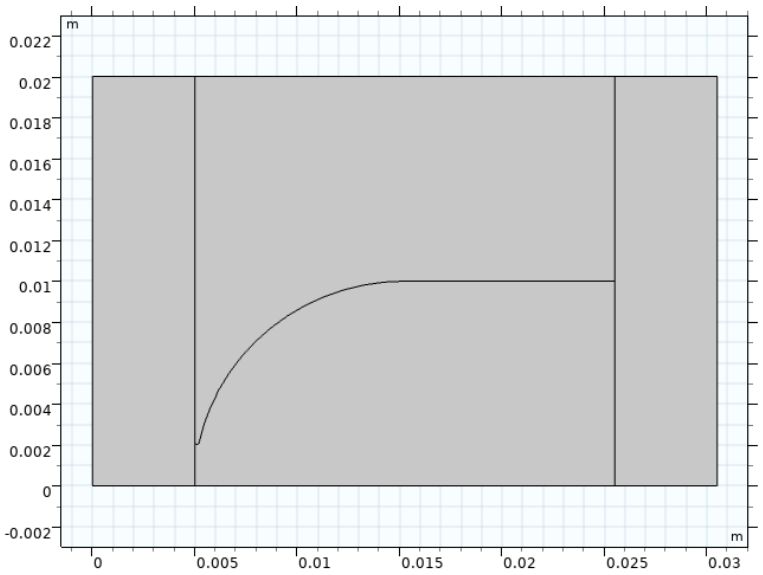

Figure 4.21: *Scaled-down geometry with smaller size and a deeper* 8 mm *wedge.*

To start with the field distribution and its impact on free charge carriers over longer simulation time will be studied. Secondly the simulation time range will be extended and several impulses will be applied. Consecutive lightning impulses are first introduced and applied without giving any longer time between the surges which excludes time for surface charge decay. Thereafter, the decays of surface charges are included for studying the behaviour and influence of charges over long simulation time. Negative polarity impulses and a lower gel height will then implemented for comparison.

4.2.2.1 Field reversal

Before introducing the consecutive lightning impulses in the simulation, some physical process after the discharge is first discussed since it may affect the motions of free charge carriers. The charge carriers will be drifted towards the interface and accumulated as surface charges which will also generate a field in the opposite direction of the background field. As the background field gradually decreasing and drifting process continuous, the surface charge generated field will be dominated at certain time after the discharge. Superimposed field direction will then be reversed resulting in different movements of the remaining free charge carriers.

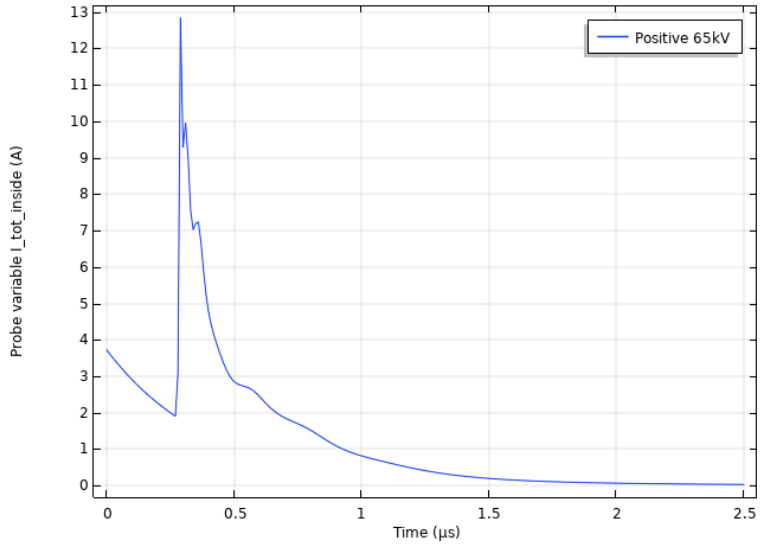

Figure 4.22: *Capacitive current under the voltage of* +65 kV.

A positive +65 kV lightning impulse is applied to the scaled-down 2D model and a discharge is initiated at around 0.29 µs from Fig.4.22. The electric field strength after the discharge is shown in Fig.4.23 where the arrows indicate the direction and magnitude of the field strength at given points.

Shortly after the discharge, the electric field in the lower region is distorted by the space charges. With the accumulation of surface charges and reduction of background field, the electric field strength is gradually reduced especially in the lower air region. If the field generated by the surface charge is large enough, the electric field will be reversed as indicated in Fig.4.23c at lower part and gradually increase in the reverse direction. As a result, the drift direction of the charge carriers will be inverted that positive and negative ions will be drifted towards the stress cone and gel surfaces respectively. The already accumulated negative surface charge on vertical surface will recombine with the newly arrived positive space charges that the surface charge concentration will then decrease.

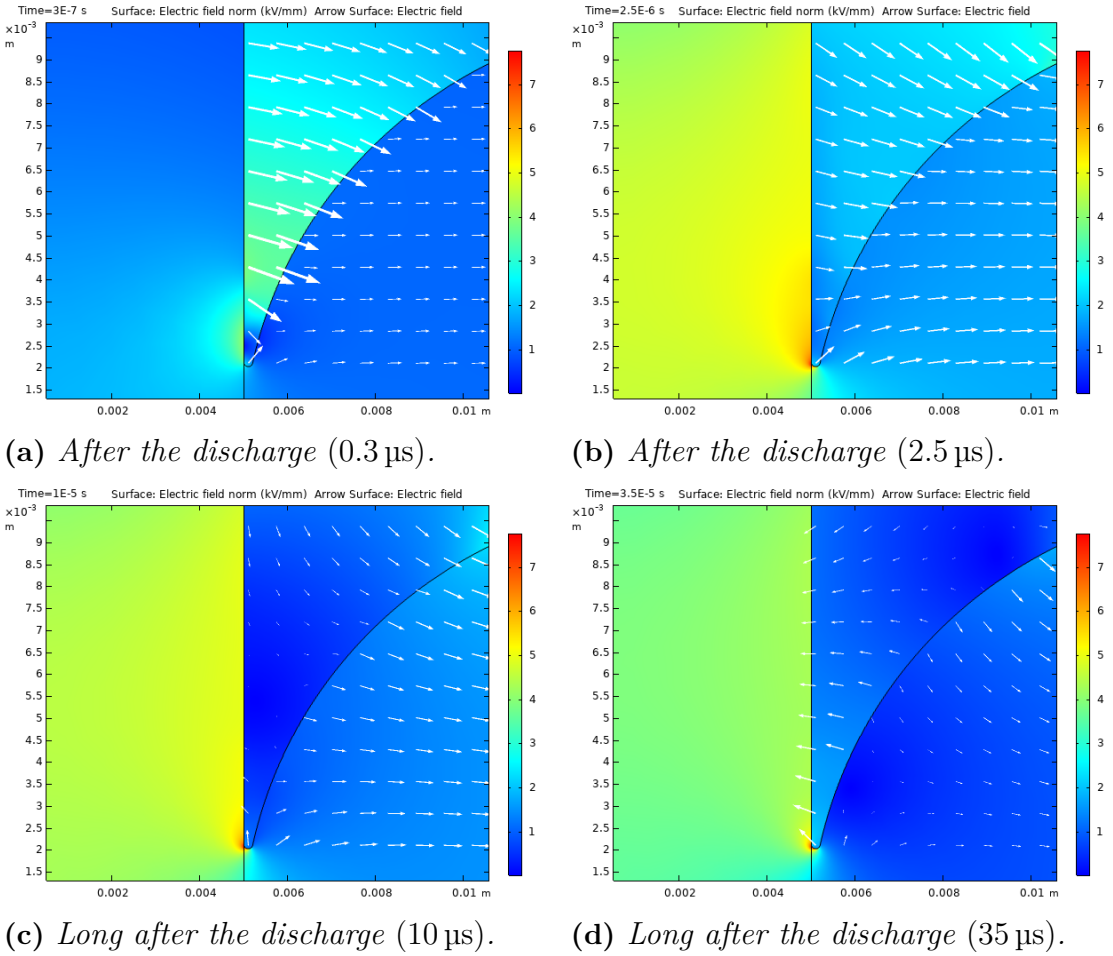

(a) *After the discharge* (0.3 µs). **(b)** *After the discharge* (2.5 µs).

(c) *Long after the discharge* (10 µs). **(d)** *Long after the discharge* (35 µs).

Figure 4.23: *Electric field strength in four time instants after the discharge under* +65 kV. *Superimposed field direction reversed after* 10 µs *which will change the drift motion of free charge carriers.*

The surface charge concentration on stress cone and gel interfaces with air until 100 µs is shown in Fig.4.24b. The x-axis parameter is the arc length starting at the top of stress cone boundary through the rounded gel corner and curved gel surface and ends at the point between flat and curved gel surfaces as shown in Fig.4.24a.

It is noted that for the top part of the vertical boundary where the background field is not greatly influenced by the charge generated field, the negative surface charge keeps accumulating. For the lower part (indicated by arc length from 0.003 m to 0.0178 m), the surface charges first increase after the discharge while gradually decrease after 10 µs due to the field reversal. The rates of increase and decrease are not identical along the boundary because of the non-uniform field and surface charge distributions. For the curved gel surface, positive surface charges are first accumulated until the field is reversed and negative ions are drifted towards the gel surface. The concentration of surface charge is then turned negative and increases in the negative direction. However at the end of curved gel interface, positive surface charges are continuously increasing since no field reversal happens at the rear region.

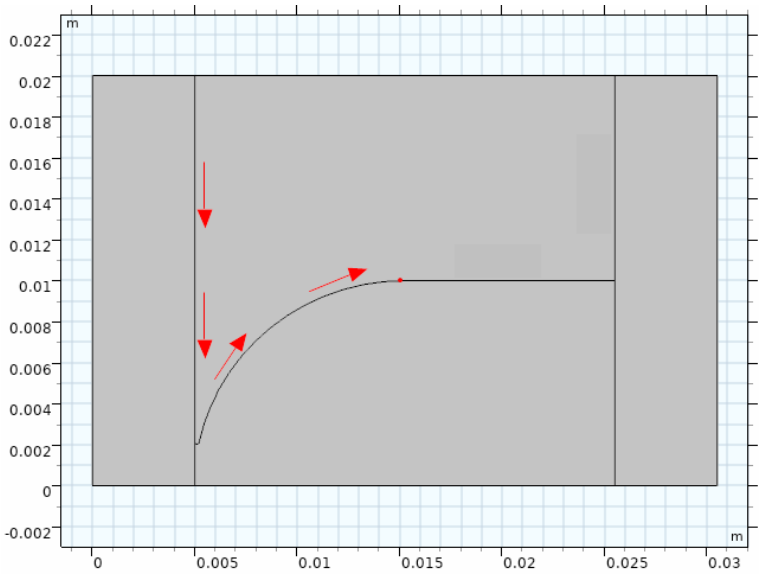

(a) *Indication of the arc length.*

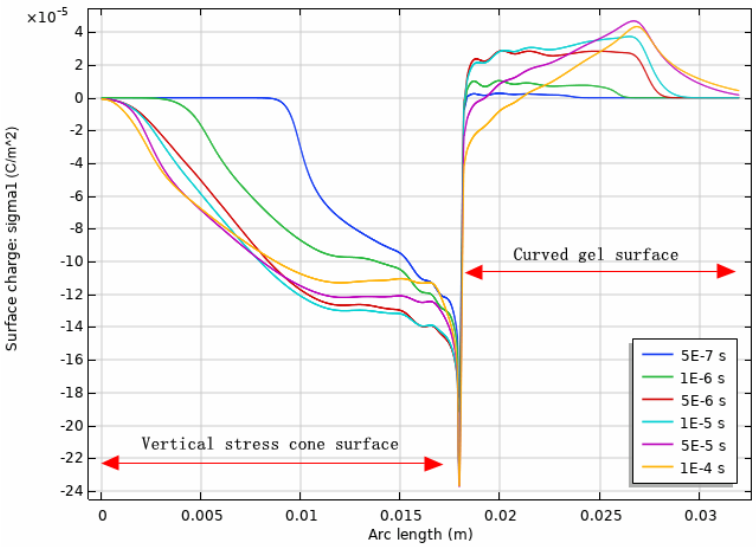

(b) *Negative surface charge on stress cone and gel surface.*

Figure 4.24: *Negative surface charge on stress cone and gel boundary until* 100 µs *under* +65 kV*. Negative surface charges on lower part of boundary first increase and then decrease due to field reversal.*

4.2.2.2 Consecutive lightning impulses

To study the charging behaviour under consecutive lightning impulses, the first option is to introduce a impulse series. The lightning impulse series is composed of three individual impulses which owns different durations and chopped at the tails. The reason for this is to save the time consumed and to minimize the effect of chopping up the tail of impulses. The electric field generated by the surface charge will be dominated after the chopping time that might result in undesired artificial ionization. Higher amount of surface charge will be accumulated with consecutive

impulses applied that such artificial influence is getting bigger. The longer durations for latter impulses are to compromise such problems by keeping the background field value to reduce the effect of surface charge generated field and avoid discharges. In addition, the sharp change of voltage derivatives between impulses will impede the convergence of the solution. A short 1 µs time gap is then added and serves as a 'relaxation' time between impulses. The used voltage shape of the consecutive impulses used in the simulations are shown in Fig.3.8 in Chapter 3.

In order to illustrate the surface charges variations during consecutive impulses, the negative surface charges on stress cone interface and the gel surface are presented for the three impulses. As can be seen in Fig.4.25, clear growths are observed since respective discharges in later impulses will generate charge carriers and later add up to the surfaces. The rounded gel corner where discharge first emerges will holds biggest increase between impulses. For higher part of vertical boundary and rare part of gel surface(left and right end of the arc), the concentration is less influenced since the electric field is lower and less influenced by the space charges.

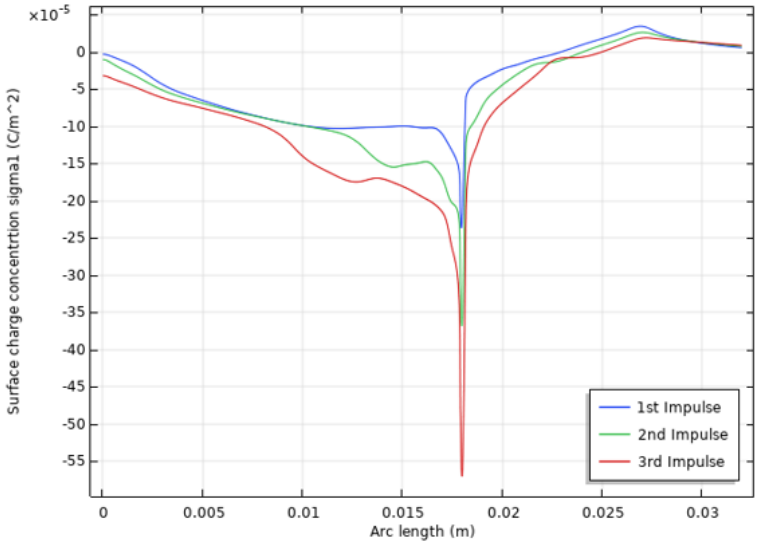

Figure 4.25: *Negative surface charges concentration on stress cone and gel boundary at the same time instant for three* +65 kV *impulses respectively. Higher amount of surface charge obtained with more impulses applied. The rate of increase is different for different part on the boundaries.*

The accumulated surface charge will have impacts on the discharging process for latter impulses. The negative surface charge concentration on curved gel surface and electric field strengths at the lowest air region at the same time instant 0.45 µs before the initiation of discharges for the second and third impulse are shown in Fig.4.26a and Fig.4.27. The remaining accumulated negative surface charges on curved gel surface will generate a electric field that enhances the background field near the curved gel surface. The enhancement increases with higher amount of negative surface charges after the second impulses as indicated in Fig.4.26a. The

higher electric field strength will result in stronger ionization in the air region that leads to more intensive discharges. The capacitive current for second and third impulses are put in the same plot in Fig.4.26b. The discharges in third impulse are more intensive compared with second impulse which is in accordance with discussion above.

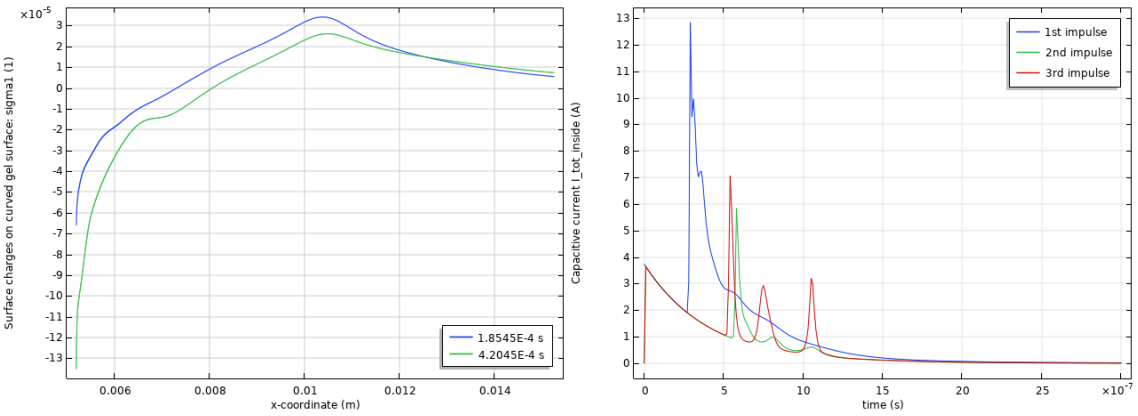

(a) *Negative surface charge.* **(b)** *Capacitive current.*

Figure 4.26: *Negative surface charge on curved gel surface at the same time instant of* 0.45 µs *and capacitive current for the second and third impulse. Discharge will be intensified with more impulses applied.*

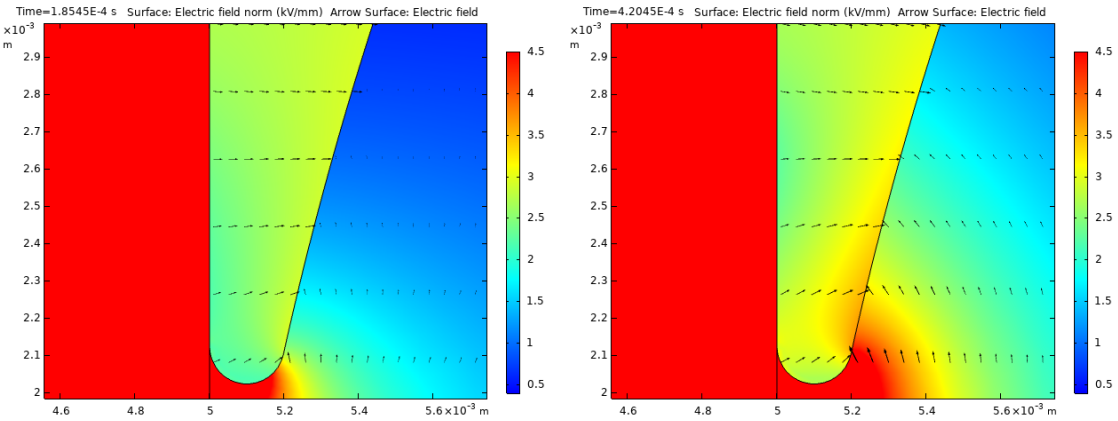

(a) *Electric field at lowest region at* 0.45 µs *for second impulse.* **(b)** *Electric field at lowest region at* 0.45 µs *for third impulse.*

Figure 4.27: *Electric field strength at the same time instant of* 0.45 µs *for the second and third impulse. The electric field strength is enhanced by the surface charge for the third impulse, resulting in more intensive discharges.*

The discussions above are based on cases with the assumptions that the decay of surface charge and space charge is rather small and thus applied the impulses in series directly to save the computational time. However during the long relaxation time between impulses in the real lightning impulse testing, the space charges concentration in air might be greatly reduced through drifting and recombination processes

and are presumed all from background ionization. Moreover, the impact of surface charge concentration on the consecutive lightning impulses has already be illustrated and thus the decay of the surface charge should be included for a comprehensive discussion.

To include the decay of surface charges, a new initial condition is employed. No remaining space charges are considered and the initial concentration are all from background ionization that $1 \times 10^{-9}\,\mathrm{mol\,m^{-3}}$ for positive and negative ions and no electrons. With the consideration of decay of surface charges, the surface charges concentration at 4500 µs is used as initial surface charge value for the consecutive impulse and then conduct the same method for another impulse. Thus three impulses in total are applied with the assumption of surface charge won't decay after 4500 µs. The reason of not choosing a longer simulation time result as initial value is the constraint of simulation power and time consumption. A study of the decay of the surface charges are supplemented in the next section to support the assumptions used.

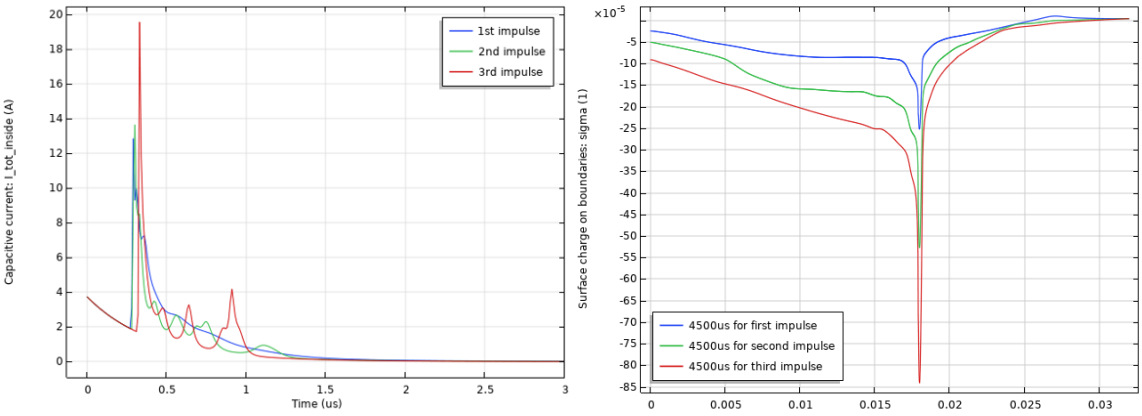

(a) *Capacitive current.* **(b)** *Surface charge concentration.*

Figure 4.28: *Capacitive current and surface charge concentration at the same time instant* 4500 µs *for three impulses.*

The capacitive currents for three impulses are shown in Fig.4.28a. Higher peak can be observed for third impulse which is in accordance with discussion in first method. Moreover, compared with Fig.4.26b, the magnitude of capacitive current is much higher. The longer simulation time and consideration of surface charge decay sustain the conclusion that the accumulated negative charges will intensify the discharges in following impulses. Nevertheless, the deviation of the results indicates that using the consecutive lightning impulse series without the consideration of decay may influence the discharge process even the result also shows a trend of intensified discharges for later impulses. This may be further improved by adjusting and fitting parameters and coefficients used in future study.

The surface charge concentrations at the last simulation time instant for three impulses are shown in Fig.4.28b. It is clear that continuous accumulations of surface charges between impulses are again observed. The rounded gel corner where

holds highest negative concentration increases to a rather high level compared with Fig.4.25 which is related to the more intensive discharges for the second and third impulses. For other part of the boundaries, the surface charge concentration is lower than compared with consecutive impulse cases. This is due to the longer simulation time that more ions will be drifted towards the boundary by the reversed field.

To sum up, the surface charges are added up with several impulse applied with or without the consideration of surface charge decay. The remaining surface charges will have impacts on follower discharges that the enhancement of background field is stronger and more rapid discharges are expected. However by applying consecutive impulses series without including the surface charge decay process, the charging dynamics can not be revealed comprehensively and certain adjustment should be made to support the conclusion better.

4.2.2.3 Surface charge decay

To support the assumptions made in last section, the decay of surface charge are discussed. The relaxation time between the lightning impulse is around 30 s in real tests which is extremely long compared with the microsecond time scale of discharging and accumulation process. Besides, the background electric field is especially low in the air region during the relaxation time that the electric field is totally dependent of the surface charge distribution. Moreover, the surface charges have impacts on charging behaviours from last section. The surface charge decay influence is necessary to inspect in this sense.

A case simulating a total of 0.4 s after discharge under +65 kV lightning impulse voltage is used to illustrate the decay of surface charge over long time. The simulation time is constrained by the demand of computational power and time. From Fig.4.29, it is noted that the surface charge concentration behaves differently for distinct boundaries. For the top part of stress cone interface and the rear side of curved gel surface, the field is very low resulting in week drifting process that surface charge concentration barely change. The rounded gel corner at the lowest region (indicated by arc length from 0.0178 m to 0.0185 m) also holds a stable surface charge concentration. This could possibly due to the low concentration of charge carriers and also tangential field direction at the lowest region. The rest of the stress cone boundary and curved gel surface have positive charges accumulated continuously causing surface charge amount reducing.

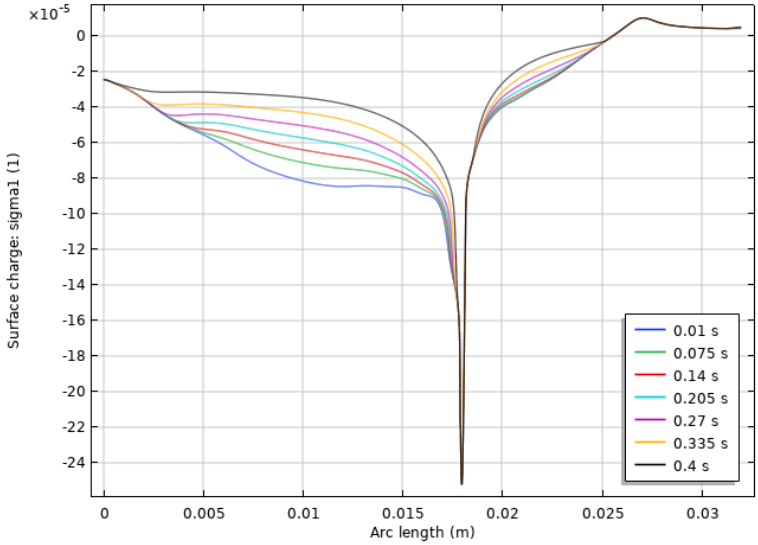

Figure 4.29: *Surface charge on stress cone and gel boundary until* 0.4 s.

Now with longer decay time considered, the influence of surface charge will again be studied to supplement the conclusion made in last section. Similar simulation method is used that the initial conditions for surface charges used now is from 0.4 s result. As shown in Fig.4.30b the decay of surface charges continues for some part of the boundary from 4500 µs to 0.4 s but the concentration at the gel corner is rather stable. In Fig.4.30a, capacitive current for first impulse, second impulse in consecutive impulses and 4500 µs and 0.4 s as initial time instants impulses are shown. It is clear that without the consideration of surface charge decay, charging behaviours in later impulses will be influenced and the results is deviated. However, the phenomenon is clear that discharges will be intensified by the surface charge even with the consideration of long decay time for surface charge. The conclusion from previous section is still valid.

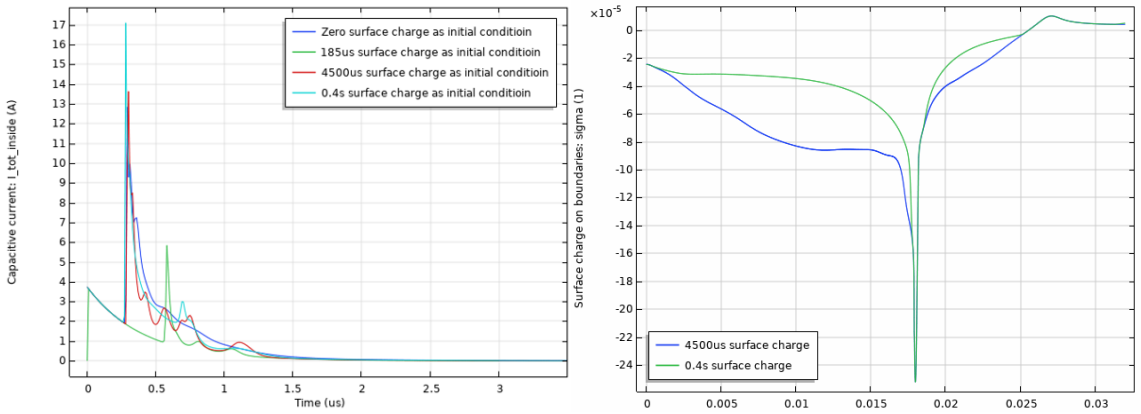

(a) *Capacitive current.* **(b)** *Surface charges.*

Figure 4.30: *Capacitive currents for cases with* 4500 µs *and* 0.4 s *surface charges as initial values. Surface charges for* 4500 µs *and* 0.4 s.

4.2.2.4 Gel height and voltage polarity

The height of the gel surface is then altered to see whether the discussion above still applicable. The gel height now is reduced to 4 mm above the contact point between the gel and the stress cone compared to the gel height of 8 mm studied in the section above. Different initial conditions is applied for three impulse that each impulse was run for 4500 µs and the surface charge concentration is used as the initial values for the following impulses. The capacitive current and the surface charge concentration at the last time instants are shown in figures below.

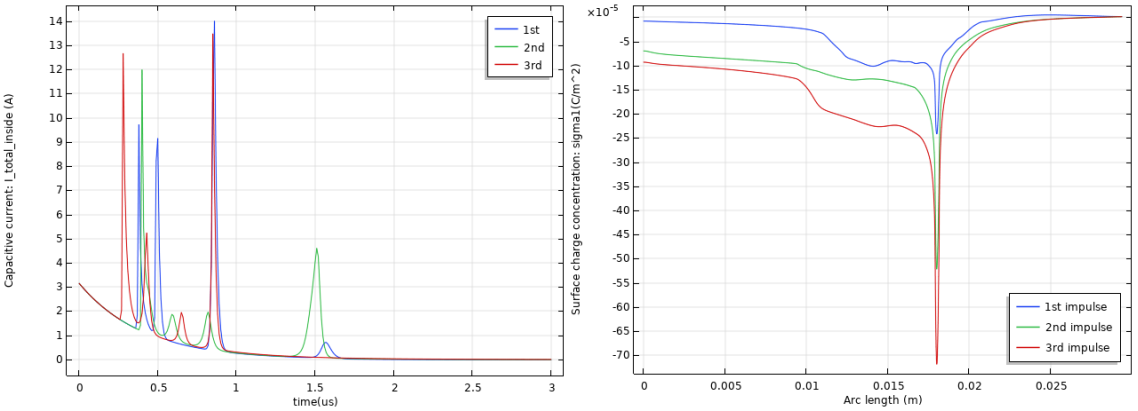

(a) *Capacitive current.* **(b)** *Surface charge concentration.*

Figure 4.31: *Capacitive current and surface charge concentration at the same time instants for three +65 kV impulses with gel height of 4 mm. The accumulated surface charge will intensify the discharges in later impulses.*

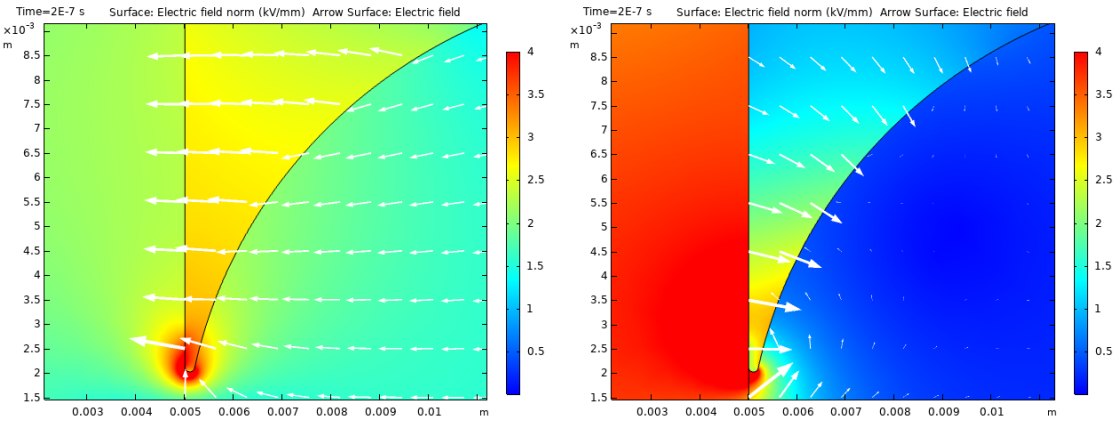

(a) *Negative polarity impulse.* **(b)** *Positive polarity impulse.*

Figure 4.32: *Electric field distribution around critical region at the same time instant (0.2 µs) for negative and positive polarity secondary impulse before the discharge. Higher electric field strength obtained for negative secondary impulse.*

As shown in Fig.4.31, the surface charge concentration increases with impulses applied. The discharges in the second and the third impulse is more intensive compared

with the first impulse, which is accordance with the results in previous case. The accumulated surface charges will altered the field distribution and intensify the discharges for later impulses. However, the onset voltage and discharge magnitude is slightly lower than higher gel surface case. This is predictable since with lower gel surface, the air region around triple junction is wider and will be stressed with lower electric field strength.

In the real lightning impulse testing, the polarity will change for the impulse voltage. As a result, the surface charge may alter the charging dynamics by a different way. A simulation is conducted with two impulses which starts from a positive polarity impulse voltage and is followed by a negative polarity impulse voltage. Each impulse voltage is applied with a duration of 4500 µs with the consideration of surface charge decay. The electric field strength in critical region is shown in Fig.4.32a . The electric field strength at a same time instant for a positive polarity second impulse in section 4.2.2.2 is shown in Fig.4.32b for comparison. As been stated the polarity effect is rather obvious that the stress cone will suffer higher electric field strength under positive polarity while gel will experience higher strength for negative polarity. The accumulated negative surface charges from the first impulse will remain on the boundaries and generate a field from right to left. When a positive polarity secondary impulse is applied, the superimposed field will be first reduced and then increased in the direction from left to right, which is the case in previous simulation.

However, when the negative polarity secondary impulse is applied instead, the superimposed field will directly increases since the background field is in the same direction with the surface charge generated field. As a result, the accumulated surface charge will act as the seed charges which results in higher field strength for a different polarity following impulse and potential failures in the system. In the same manner, if a negative polarity impulse is first applied and followed by a positive secondary discharge, the resulted electric field strength will be higher and the risk for a strong localized discharge is much higher. Thus the polarity reversal increases the risk for a propagating streamer discharge or even an partial breakdown between the stress cone and the insulator. These phenomena are however not included in this study.

4.2.2.5 Conclusion

Additional understandings on the discharge dynamics and surface charge decay in the context of multiple consecutive LI surges are obtained in this subsection . Some of the main findings are summarized as follow:

1. A certain time after a discharge (during the decline of the voltage surge) the electrical field in the region nearby the discharged area changes direction and are opposite to the background field. This is the effect of the charges deposited on the polymer surfaces.
    - The reversed field direction will cause remaining space charge to move towards surfaces in an opposite direction and the surface charge will decay over time.

- At most part of the surfaces the decay continues over time and after 0.4 s the majority of the surface charges have diminished. However the surface decay effect is limited deep down in the air wedge. This is most likely due to the small air volume and the limited number of ions that could contribute to the decay process.

2. Consecutive LI have an impact on the discharges due to remaining surface charges.
   - With a very short time gap between impulse surges, the discharges in later impulses are intensified and occur earlier for each surge.
   - With longer time between the impulses, the effect becomes less pronounced. Nervelessly, even with 0.4 s between the pulses a detectable difference occurs.

3. In order to get a better understanding of the surface charge decay process and its impact on the discharges with consecutive LI, further detailed studies is needed. Since it does not fit into the time frame of the present master thesis work a few things that need further investigations are proposed:
   - Detailed analysis of the space charge and electrical field distribution during the consecutive LI surges.
   - Validation of the surface charge decay rate against experimental results. Sensitive study on how the parameters such as recombination rates and the electrical mobilities of the charge carriers affect the simulation results [16].

4.3 Discussion and interpretation

In this section the discussion and interpretation of the main results are summarised for better understanding.

1. The three solids and two air gaps 1D model is used to represent the critical region around the gel surface and used to illustrate basic corona discharge dynamics.
   - Under lightning impulse voltage, a corona discharge emerges in domain 1 under +80 kV and intensified with higher voltage level. The higher voltage level will result in higher electric field strength in domain 2 and lead to a secondary discharge.
   - The transport of space charges in the air domain is accompanied with surface charges accumulation. The positive surface charges are collected on gel surface and negative surface charges are accumulated on stress cone surface in domain 1.
   - The isotropic diffusion stabilization method used has been proven useful to resolve the high concentration gradient problem and reduce the non-physical behaviour. However, the artificial diffusion will affect the accuracy of the result.

2. The 2D model with one air wedge is utilized for demonstrating the charging behaviour in the critical air region.
   - Under positive polarity, the corona discharge will develop along the vertical stress cone boundary due to the local field enhancement by the positive ions. The positive ions will then be drifted away from the stress cone and accumulate on gel surface while the negative ions will be attracted and collected on the vertical stress cone surface. The stress cone near the discharged area will suffer from high field strength.
   - With higher voltage level or higher gel surface, the critical air region will be stressed even further that the discharge is intensified and covers bigger region.
   - Under negative polarity, the discharge develops along curved gel surface and the gel is stressed with higher electric field strength compared with positive case.

3. The scaled-down 2D geometry is applied to investigate the charging behaviour over long simulation time.
   - Field reversal in critical region due to the surface charges generated field is observed after the discharge. As a result, the surface charges concentrations on part of the boundaries are reduced due to the decay over time.
   - Under consecutive lightning impulses, the accumulated surface charges are superimposed and results in higher amount of surface charges concentration. The discharges at later impulses are thus influenced by the accumulated negative surface charge on gel surface and will be intensi-

fied. In others words, the discharge withstand ability is reduced because of the collected surface charge. However, these results overestimate the size of the discharges since no surface charge decay is considered.
- The decay of surface charges is included using a different initial condition. The intensification of discharges by the accumulated surface charges is confirmed under relative long simulation time range.
- Higher electric field strength will be obtained if the following impulse holds different polarity.
- Charge decay over time will affect the impact of consecutive LI surges. However, the charge decay in the most narrow part deep down in the air wedge is much less affected by surface charge decay. Most likely because of limited amount of ions in the nearby air volume.

4. A number of uncertainties due to the limitations of the used physical model exist.
   - Precision of the calculated surface charge decay over time partly due to the uncertainty of the used input parameters.
   - No physical model for de-trapping of surface charge nor surface transport is implemented [17]. The used physical model is not able to resolve any self-propagating discharges.

5
Conclusion

5.1 Main findings

This study has investigated the charging behaviours under lightning impulses in simplified geometries reflecting the critical region around the gel surface in dry-type air insulated cable terminations. The corona discharge dynamics have been illustrated while the charges transport and accumulation have been studied carefully. The effects of surface charge on charging dynamics are discussed and the decay of surface charges are studied in the range of computational ability.

Nevertheless, some aspects of the simulation can be improved but was not reached in this work due to the constraints of time and computational power. Firstly, only the 2D model with one air wedge is considered in the simulation. Secondly, the coefficients and parameters used are from previous work which requires fitting and adjustment for more accurate results. Thirdly, the study on decay of surface charges is constrained by the computational power and time. Last but not least, the results hold large uncertainty since no comparable experimental results are available.

5.2 Future work

Some interesting points that can be further studied are illustrated:

- Sensitive analysis on parameters and coefficients should be carried out based on the experimental work.
- The study of charging behaviours based on two air wedge geometry or coaxial system can be carried out. The study can even be extended further to simulate the real product system.
- The mesh influences on the results can be studied especially for smaller element sizes around 10 µm level in critical area.
- The decay of surface charges can be investigated thoroughly given longer simulation time and detailed comparison with experimental results.
- A trapping-detrpping physics on the boundary can be included for a more comprehensive studied.
- A model for charge transport at the polymer interfaces could be formulated and implemented.
- A simplified criterion for a self-sustaining streamer propagation could be formulated based on the field created by the discharges with the present model.

Bibliography

[1] G. Karman, "Simulation and analysis of corona currents in large scale coaxial geometry due to triangular voltages," Master's thesis, Chalmers University of Technology, Gothenborg, 2013.

[2] M. Macken, "Modelling and simulations of corona discharge currents in a large scale coaxial geometry with a dielectric barrier due to low frequency triangular voltages," Master's thesis, Chalmers University of Technology, Gothenborg, 2014.

[3] A. Küchler, *High Voltage Engineering*. Schweinfurt: Springer Vieweg, 2018.

[4] R. Waters and W. Stark, "Characteristics of the stabilized glow discharges in air," *Journal of Physics D: Applied Physics*, vol. 8, p. 416, 01 2001.

[5] G. N. T. Farouk A.M. Rizk, *High Voltage Engineering*. Boca Raton: CRC Press, 2014.

[6] J. Shea, "Gaseous electronics - theory and practice [book review]," *Electrical Insulation Magazine, IEEE*, vol. 22, pp. 53–53, 12 2006.

[7] E. Kuffel, "Electron attachment coefficients in oxygen, dry air, humid air and water vapour," *Proceedings of the Physical Society*, vol. 74, p. 297, 12 2002.

[8] S. McGowan, "Ion-ion recombination in laboratory air," *Physics in Medicine and Biology*, vol. 10, no. 1, pp. 25–40, jan 1965.

[9] G. Braglia, "The diffusion and drift of electrons in gases a monte-carlo simulation," *Physica B+C*, vol. 92, no. 1, pp. 91 – 112, 1977.

[10] S. Kumara, Y. V. Serdyuk, and S. M. Gubanski, "Simulation of surface charge effect on impulse flashover characteristics of outdoor polymeric insulators," *IEEE Transactions on Dielectrics and Electrical Insulation*, vol. 17, no. 6, pp. 1754–1763, 2010.

[11] W. N. English, "Positive and negative point-to-plane corona in air," *Phys. Rev.*, pp. 170–178, Jul 1948.

[12] L. B. Loeb, *Electrical coronas, their basic physical mechanisms*. University of California Press, 1965.

[13] V. Ivanov, K. Klopovsky, D. Lopaev, A. Rakhimov, and T. Rakhimova, "Experimental and theoretical investigation of oxygen glow discharge structure at low pressures," *Plasma Science, IEEE Transactions on*, vol. 27, pp. 1279 – 1287, 11 1999.

[14] G. Raju, *Gaseous electronics: Theory and practice*, 2005.

[15] N. Babaeva, J. Lee, and H. Kim, "Non-stationary charging of a dust grain in decaying streamer-channel plasma," *Plasma Sources Science and Technology*, vol. 13, p. 127, 2003.

[16] S. Sato, W. S. Zaengl, and A. Knecht, "A numerical analysis of accumulated surface charge on dc epoxy rrsin spaces," *IEEE Transactions on Electrical Insulation*, vol. EI-22, no. 3, pp. 333–340, 1987.

[17] F. Zhou, J. Li, Z. Yan, X. Zhang, Y. Yang, M. Liu, D. Min, and S. Li, "Investigation of charge trapping and detrapping dynamics in ldpe, hdpe and xlpe," *IEEE Transactions on Dielectrics and Electrical Insulation*, vol. 23, no. 6, pp. 3742–3751, 2016.

A

Appendix

Table A.1: Geometry parameters used in the simulation model

Description	Name	Value
1D model		
Stress cone length	L_stress	0.02m
Air gap 1 length	L_air_1	0.005m
Gel length	L_gel	0.035m
Air gap 2 length	L_air_2	0.005m
Insulator length	L_ins	0.0125m
2D geometry		
Width of the set up	W_setup	0.0605m
Width of the stress cone	W_solid1	0.005m
Width of the insulator	W_solid3	0.005m
Height of the set up	H_cell	0.01m
Height of the gel	H_solid2	0.003m
Fillet radius	R_1	0.04m
2D scaled down geometry		
Width of the set up	W_setup	0.035m
Width of the stress cone	W_solid1	0.005m
Width of the insulator	W_solid3	0.005m
Height of the set up	H_cell	0.02m
Height of the gel	H_solid2	0.01m
Fillet radius	R_1	0.001m

Table A.2: Constant parameters used in the simulation model

Description	Name	Value
Boltzmann's constat	kb	1.3806488e-23 J/K
Elementary charge	q	1.6000432e-19C
Permittivity of vacuum	eps0	8.85418781e-12 F/m
Background ionization rate	R0	1.7e-7 1/m^3s
Electron-ion recomb. rate	beta_ei	5e-14 m^3/s
Initial ion concentration	n0	1e9 m^-3
Mass of electron	m_e	9.109383e-31 kg
Mass of O_2^- ion	m_n	5.3e-26 kg
Mass of O_2^+ ion	m_p	$m_g - m_e$
Mass of O_2 molecule	m_g	$m_n - m_e$
Mobility of negative ions	mu_n	2.0e-4 m^2/Vs
Mobility of positive ions	mu_p	2.7e-4 m^2/Vs
Secondary emission coeffiecient	gamma	1e-3
Actual pressure	pg	101325 pa
Actual temperature	Tg	293 K
Relative air density	delta	1
Gas density	N	2.5055e25 1/m^3
Tuning parameter	ad_p	0.5
Voltage amplitude	u_amp	80 kV

Table A.3: Variables used in the simulation model

Description	Name	Expression
Diffusion coeff.electrons	D_e	Dmu_e(EN_td)*mu_e
Diffusion coeff.pos.ions	D_p	mu_p*kb*T_p/q
Diffusion coeff.neg.ions	D_n	mu_n*kb*T_n/q
Space charge density	rho	q*(mod1.pos-mod1.neg-mod1.e)
Source term electrons	source_e	Rion+R0+Rdet+Rrec_ei-Ratt
Source term positive ions	source_p	Rion+R0-Rrec_ei-Rrec_ii
Source term negative ions	source_n	Ratt-Rdet-Rrec_ii
Detachment coefficient	k_det	2.5e-19*exp(-6030/T_n)
Detachment frequency	nu_det	k_det*N
Detachment rate	Rdet	max(eps^2,nu_det*mod1.neg)
Ion-ion recomb.coeff.	beta_ii	1.5e-12*sqrt((300/T_p)*(300/T_p)*(300/T_p))
Ion-ion recomb.rate	Rrec_ii	max(eps^2,beta_ii*mod1.pos*mod1.neg)
Ion-electron recomb.rate	Rrec_ei	max(eps^2,beta_ei*mod1.ele*mod1.pos)
Reduced electric field	EN_td	abs(mod1.es.normE)/N*1e21
First ionization coeff.	alpha	N*alphaN(EN_td)
Attachment coeffcient	eta	N*etaN(EN_td)
Attachment rate	Ratt	max(eps^2,eta*mod1.ele*W_e(EN_td))
Ionization rate	Rion	max(eps^2,alpha*mod1.ele*W_e(EN_td))
Electron mobility	mu_e	(W_e(EN_td)/abs(mod1.es.normE))*(abs(mod1.es.normE)>0)
Neg.ion temp.	T_n	tg+(m_n+m_g)*((mu_n*abs(mod1.es.normE))^2)/kb/3
Pos.ion temp.	T_p	tg+(m_p+m_g)*((mu_p*abs(mod1.es.normE))^2)/kb/3